RESEARCH ARTICLE

A gradient of the HD-Zip regulator Woolly regulates multicellular trichome morphogenesis in tomato

MinLiang Wu[1, †], XinXin Bian[1, †], ShouRong Hu[1, †], BenBen Huang[1], JingYuan Shen[1], YaDi Du[1, 2], YanLi Wang[1, 2], MengYuan Xu[1], HuiMin Xu[1], MeiNa Yang[1], Shuang Wu[1, *]

1. College of Horticulture, College of Life Sciences, Haixia Institute of Science and Technology, Fujian Agriculture and Forestry University, Fuzhou 350002, China.
2. College of Life Sciences, Fujian Agriculture and Forestry University.

† These authors contributed equally

Short title: Regulation of tomato trichome morphogenesis

* Corresponding Author: Shuang Wu (wus@fafu.edu.cn)

The author responsible for distribution of materials integral to the findings presented in this article in accordance with the policy described in the Instructions for Authors (https://academic.oup.com/plcell/pages/General-Instructions) is: Shuang Wu (wus@fafu.edu.cn).

Abstract

Homeodomain (HD) proteins regulate embryogenesis in animals such as the fruit fly (*Drosophila melanogaster*), often in a concentration-dependent manner. HD-leucine zipper (Zip) IV family genes are unique to plants and often function in the L1 epidermal cell layer. However, our understanding of the roles of HD-Zip IV family genes in plant morphogenesis is limited. In this study, we investigated the morphogenesis of tomato (*Solanum lycopersicum*) multicellular trichomes, a type of micro-organ in plants. We found that a gradient of the HD-Zip IV regulator Woolly (Wo) coordinates spatially polarized cell division and cell expansion in multicellular trichomes. Moreover, we identified a TEOSINTE BRANCHED1, CYCLOIDEA, and PROLIFERATING CELL NUCLEAR ANTIGEN BINDING FACTOR (TCP) transcription factor-encoding gene, *SlBRANCHED2a* (*SlBRC2a*), as a key downstream target of Wo that regulates the transition from cell division to cell expansion. High levels of Wo promote cell division in apical trichome cells, whereas in basal trichome cells, Wo mediates a negative feedback loop with SlBRC2a that forces basal cells to enter endoreduplication. The restricted high and low activities of Wo patterns the morphogenesis of tomato multicellular trichomes. These findings provide insights into the functions of HD-Zip IV genes during plant morphogenesis.

Key word: Multicellular trichome morphogenesis; HD-Zip transcription factor; Dosage dependent regulation; Endoreduplication; SlBRC2a

Introduction

Morphogenesis is a fundamental process of plant development involving the spatial organization of cell division and cell expansion within a tissue (Donnelly et al., 1999). Pioneering genetic studies in the fruit fly (*Drosophila melanogaster*) uncovered the key role of homeodomain proteins in determining the body plan (Gehring et al., 1994). Knockdown or overexpression of any of these homeobox domain genes can cause homeotic transformation of the corresponding tissues or organs (Jegalian and De Robertis, 1992; Grammatopoulos et al., 2000). Interestingly, many regulators that control tissue patterning are iteratively deployed during the progressive developmental processes, and thus often act in a concentration dependent manner (Perrimon et al., 2012; Sagner and Briscoe, 2017). The term of morphogen was coined by Alan Turing in 1952 to explain the control of tissue patterning by the gradient of the key molecules (Turing, 1990; Anirban, 2022). It is thought that most of the developmental cues act as morphogens, over a distance within a tissue, to govern tissue patterning. This leads to the idea that different concentrations of morphogens will trigger distinct downstream transcriptional programs in different receiving cells. Therefore, interpreting the concentration-dependent regulators that convey positional information is key to understanding tissue patterning and organogenesis.

HD-Zip IV family genes, although containing homeobox domains, are unique to plants (Ariel et al., 2007). Despite the sequence divergence, HD-Zip IV genes have often been found to control the spatial arrangement of cell types in plant development. Interestingly, many HD-Zip IV genes are mainly expressed and function in L1 layer and epidermal cells (Abe et al., 2001; Rombola-Caldentey et al., 2014; Sun et al., 2020). In Arabidopsis, the HD-Zip IV protein HOMEODOMAIN GLABROUS2 (HDG2) is involved in the regulation of stomatal cell differentiation (Peterson et al., 2013); ARABIDOPSIS THALIANA MERISTEM LAYER1 (AtML1) regulates the giant cell formation in the sepal epidermis (Roeder et al., 2012). GLABRA2 (GL2) is a key regulator of root hair and unicellular trichome formation (Di Cristina et al., 1996; Szymanski et al., 1998; Ohashi et al., 2002). Interestingly, AtML1 has been shown to regulate the developmental processes in a concentration dependent manner (Meyer et al., 2017; Hong et al., 2023). However, it is not clear whether this is a common activity feature of the HD-Zip IV regulators.

Plant organogenesis usually follows a stereotypical track, with cell division followed by cell

expansion and differentiation (Ioio et al., 2008; Zhang et al., 2023). To dissect the developmental principles during organogenesis, it is convenient to have a simple and tractable system to study. In plants, single-cell trichome has been widely studied to address the principles of plant morphogenesis (Szymanski et al., 1999; Wolpert et al., 2000; Deeks et al., 2004; Hülskamp, 2004; Zhang et al., 2008; Yanagisawa et al., 2015). However, about 30% of vascular tissues produce multicellular trichomes (Glas et al., 2012). The simple nature of the patterning and anatomy of the multicellular trichomes, as well as the feature of protrusion above the surface, make them an ideal system for studying organ morphogenesis.

In tomato, multicellular trichomes develop into seven types of trichomes (named I–VII) with different morphologies and functions (Simmons and Gurr, 2005). The HD-Zip IV gene, *Woolly* (*Wo*) has been shown to control a wide range of developmental events during tomato trichome formation, from trichome initiation to fate determination of different types of trichomes (Yang et al., 2011; Wu et al., 2023b). Intriguingly, Wo specifies different trichome fates also in a concentration dependent manner, with high concentrations favoring non-glandular trichomes while low concentrations promoting glandular trichomes (Wu et al., 2023b). Since the distinctive morphological features are the direct result of the cell fate determination, it is important to know how Wo steers the morphogenesis of multicellular trichomes.

In this study, using multicellular trichomes in tomato, we found the morphogenesis of tomato trichomes consists mainly of two spatially polarized processes: cell division in apical cells and cell expansion in basal cells. The Wo gradient along the trichome axis spatially patterns the cell division and endoreduplication that drives basal cell expansion. We further identified a Wo downstream gene, a TEOSINTE BRANCHED1, CYCLOIDEA, and PROLIFERATING CELL NUCLEAR ANTIGEN BINDING FACTOR (TCP) transcription factor *Solanum lycopersicum BRANCHED2a* (*SlBRC2a*), that functions to promote the transition from the cell division to endoreduplication in tomato trichomes. Although activated by Wo, SlBRC2a in turn binds to Wo and inhibits the transcriptional activity of the Wo, forming a negative feedback loop of the Wo pathway. Interestingly, the expression of *SlBRC2a* also exhibits a spatial gradient, with higher levels in basal cells while no detectable expression in apical cells. This restricted Wo-mediated cell division to the apical cells, resulting in the polarized pattern of cell division in the apical region of the trichomes. Our results reveal the key role of Wo and its downstream gene *SlBRC2a* in

tomato trichome morphogenesis and our finding of the Wo-SlBRC2a negative feedback loop also provides insights into the function of HD-Zip IV transcription factors.

Results

1. Spatially polarized arrangement of cell division and endoreduplication in tomato trichomes

Different patterns of cell division and cell differentiation give rise to seven types of trichomes with different morphology and functions in tomato (Fig. 1A). Digital trichome (DT) usually has multiple stalk cells whereas peltate trichome (PT) has only one stalk cell. Thus, the number of stalk cells and the length of the trichomes were positively associated (Fig. 1B). Using the histone H2B-GFP fusion protein system (*pro35S:H2B-GFP*) (Chang et al., 2021), we observed the spatial distribution of the cell division along the trichome cell files. Our observation and quantification indicated that the cell division generating the variable number of stalk cells, was restricted to the apical cells (Fig. 1C-H). A regular long trichome such as type I or II trichomes could undergo about ~5-8 rounds of cell division, but the majority of PT experienced only one division in their stalks (Fig. S1A).

Temporally, tomato trichomes underwent interactive cell division prior to the spatially polarized cell division and cell expansion along the trichome cell file. In the early stages of trichome morphogenesis, the nucleus size of apical and basal cells was similar (around 4C) (Fig. 1I-J). As trichome morphogenesis progressed, basal cells underwent pronounced endoreduplication as well as cell expansion, whereas apical cells gradually ceased cell division, resulting in the final mature long conical multicellular trichomes (Fig. 1I-J). These observations suggest that the regulation of trichome morphogenesis is a spatiotemporally ordered process. Interestingly, the mature basal cells in tomato trichomes (typically in type I and II trichomes) were much larger in size than the unicellular trichomes in Arabidopsis (Fig. S1B). In line with this observation, the polyploidy state of these basal cells was substantially greater than that of Arabidopsis trichomes, reaching as high as 96 C (Fig. 1I-J, Fig. S1 C-D).

2. Wo protein gradients are associated with discrimination of cell division and cell expansion

Our previous results have shown that Wo determines different fates of trichomes in a concentration-dependent manner (Wu et al., 2023b). A key morphological feature that distinguishes different trichomes is the different patterns of cell division in different types of trichomes (Fig. 1C-H, Fig S1A). Interestingly, observation of Wo-GFP in individual cells along the trichome cell file showed that Wo-GFP levels were positively associated with the division capacity (Fig. 2A), and almost disappeared in the stalk of PT when the differentiation started after a single cell division (Fig S1E-F). In type IV and V, which have only 2-3 cells in the stalk, Wo-GFP gradually reduced after several rounds of cell division. In contrast, in type I or II, whose stalk contains 6-8 cells, Wo-GFP levels remained at a high level even after several rounds of cell division (Fig. 2A). These results suggest that the division capacity of trichome cells is associated with high levels of Wo protein.

To test this hypothesis, we took advantage of the mutants in which Wo proteins become stabilized and thus the Wo protein levels are elevated. In the previously reported E3-ligase mutants *Multicellular Trichome Repressor 1* (*MTR1*) and *Multicellular Trichome Repressor* 2 (*MTR2*), we found that Wo protein levels were dramatically increased (Wu et al., 2020; Wu et al., 2023b). In these mutants, long digital trichomes were substantially increased, possibly generated through promoted cell division (Fig. 2B). Quantification indicated that long digital trichomes (type I-III) were increased 10-fold in the mutants with elevated Wo protein levels (Fig. 2C). However, the dividing capacity of the apical cells appears to be tightly controlled, as the high expression of *MTR1* and *MTR2* in the apical cells of the developing trichomes (Fig. 2D) fine-tunes Wo levels in these cells.

Digital trichomes have multiple cells in their stalk, and thus they are a better system for testing the spatial organization of cell division and cell expansion. In the early stage of these two types of trichomes, Wo protein concentration in the apical cells was significantly higher than that in the basal cells (Fig. 2E-F). Wo proteins were maintained at a high level in the apical cells until the dividing capacity faded away. These results suggest that high Wo protein level may promote cell division in apical cells.

To test this, we expressed gain-of-function mutant alleles Wo^{P635R} and Wo^{V} (Fig. S2A-B), which confer significantly enhanced Wo protein stability (Fig. 3A-C), from its native promoter and the DT specific promoter *MIXTA-like 1* (*MX1*, *proMX1:*Wo^{V}*-GFP*). An advantage of using *MX1*

promoter is that it avoids the potential embryo lethality caused by the *Wo* promoter (Fig. S2C-D). In developing trichomes, more stable Wo proteins led to increased cell division (Fig. 3C, Fig. S2E-F). In more mature trichomes, cell division, as shown in *proMX1:Wo^{V}-GFP* transgenic lines, was substantially increased compared to WT (Fig. 3D), resulting in 2C nuclei in almost all trichome cells (Fig. 3E). This indicates that high Wo protein concentration is essential and sufficient to induce cell division in tomato trichomes. It is likely that high Wo level in apical cells during the early stage of trichome morphogenesis maintains active mitosis in the apical region, whereas reduced Wo levels in basal cells may account for the transition from cell division to cell expansion in this region (Fig. 3F).

3. SlBRC2a is a key regulator of the shift to cell expansion in basal cells

To elucidate how decreased Wo levels in basal cells could lead to a shift towards cell expansion, we screened for Wo downstream genes by comparing the differentially expressed transcription factors in the gain-of-function mutant *Wo^{P635R}* and the loss-of-function mutant *wo^{W106R}* (Wu et al., 2023b). Among them, *SlBRC2a*, a member of the CYC/TB1 TCP family, exhibited a highly differential expression pattern in *Wo* mutants (Fig. 4A). Phylogenetic analysis revealed that SlBRC2a is a BRC-like protein (Fig. S3). To visualize the spatial expression pattern of *SlBRC2a,* we generated transcriptional and translational reporter lines (*proSlBRC2a:GFP-GUS* and *proSlBRC2a:SlBRC2a-GFP*) using its native promoter (3000 bp upstream of the ATG). In both lines, *SlBRC2a* displayed a gradient expression pattern, with highest level in the basal cells of tomato trichomes (Fig. 4B-C).

To study SlBRC2a function, we generated loss-of-function mutants of *SlBRC2a* using CRISPR-Cas9 (*cr-slbrc2a*, Fig. S4A-C). The *SlBRC2a* mutants showed a significantly increased trichome density (Fig. S4D-E) and cell division in long digital trichomes (type I/II) (Fig. 4D-E). Furthermore, the increased division capacity was not restricted along the trichome cell file, instead, some cells showed the lateral division, resulting in forked and branched trichomes, which was never found in WT (Fig. 4F-G). We further examined the nucleus size using *pro35S:H2B-GFP* marker line. In the *cr-slbrc2a* mutant background, the nucleus size in basal trichome cells shown by *pro35S:H2B-GFP*, was significantly smaller than that in WT (Fig. 4H-I, Fig. S4F). Therefore, SlBRC2a is essential for the transition from cell division to endoreduplication

and cell expansion in basal trichome cells.

4. SlBRC2a inhibits cell division in trichomes

Next, we selected stem tissues close to the SAM region where cell division is active for transcriptome analysis. Interestingly, the expression pattern of differentially expressed transcription factors in *cr-slbrc2a* and *cr-wo* mutants (Wu et al., 2023b) was almost opposite (Fig. 5A-B, Suppl. data set S1). Among these genes, we found *MX1*, a key gene for Wo-mediated regulation of DT differentiation (Wu et al., 2023b). We further validated the expression change of *MX1* in the *cr-slbrc2a* mutant by RT-qPCR (Fig. 5C). This suggests that SlBRC2a may function as a negative regulator of the Wo protein. To test this, we crossed the *cr-slbrc2a* mutant with the gain-of-function mutant Wo^{P635R} (cr-*slbrc2a* × Wo^{P635R}). As shown in Fig. S5, cr-*slbrc2a* × Wo^{P635R} mutants had markedly increased cell division in the trichome stalk and trichome cells became smaller compared with Wo^{P635R}, suggesting that *SlBRC2a*, which is genetically epistatic to *Wo*, can repress Wo ability to promote cell division.

To fully dissect the relationship between the Wo and *SlBRC2a*, we knocked out *SlBRC2a* in the *proWo:Wo-GFP* background (*cr-slbrc2a* × *proWo:Wo-GFP*). In WT, Wo-GFP fluorescence in basal cells was significantly reduced after the early stage of cell division (Fig.2E-F). However, in the *cr-slbrc2a* × *proWo:Wo-GFP* plants, Wo-GFP appeared to be increased in the basal cells and Wo-GFP bearing nucleus often moved towards the side wall where additional cell division was about to occur (Fig. 5D-G). *cr-slbrc2a* × *cr-wo* double mutants exhibited *cr-wo* single mutant phenotype, suggesting the epistasis of *SlBRC2a* to *Wo* (Fig. S6A). However, *Wo* expression became elevated in *cr-slbrc2a* mutant (Fig. S6B), which may account for the increased cell division in *cr-slbrc2a* trichomes.

5. SlBRC2a negatively affects Wo transcriptional activity

Previous studies suggest that TCP proteins often interact with other transcription factors to regulate the expression of downstream genes (Martín-Trillo and Cubas, 2010). The genetic and transcriptomic data all suggest that SlBRC2a antagonizes Wo activity. To further address this, we examined the protein interaction between these two transcription factors. Co-IP, yeast two-hybrid, and BiFC methods all showed that the Wo protein indeed interacted with the SlBRC2a protein

(Fig. 6A-C, Fig. S6C-D). The yeast one-hybrid result showed that the yeast cells carrying the *SlBRC2a-pJG4-5* and *proMX1-pLacZi* plasmids barely turned blue in the screening medium, indicating no direct interaction between the SlBRC2a and the *MX1* promoter (Fig. 6D). Although SlBRC2a did not bind directly to the *MX1* promoter, our LUC reporter assay showed that SlBRC2a was able to represses the ability of Wo to upregulate the expression of *MX1*, as well as several other Wo downstream genes (Fig. 6E-F, Fig. S7A-B). It is likely that SlBRC2a binds to the Wo protein to interfere with its ability to activate downstream genes.

Based on above results, we hypothesized that the increased cell division in the *cr-slbrc2a* mutant was caused by up-regulation of Wo downstream genes. To test this, we simultaneously knocked out *MX1* gene, which was the most significantly up-regulated gene in the transcriptome data, in the *cr-slbrc2a* mutant. As expected, knockout of the *MX1* gene resulted in declined cell division in both type I and II trichomes (Fig. 6G-H). Compared to *cr-slbrc2a*, we also found that the number of PT trichomes was significantly increased in the *cr-mx1*× *cr-slbrc2a* mutant (Fig. S7C).

To further test whether SlBRC2a negatively affects Wo activity, we crossed *cr-slbrc2a* and *mtr1 mtr2.* Compared with *mtr1 mtr2* double mutant, the triple mutant had marked increase of cell division in trichomes as well as trichome density (Fig. 7A-E, Fig. S8A-C). In *SlBRC2a* overexpression lines (*OE-SlBRC2a, CaMV 35S* promoter), we observed a significantly reduced trichome density compared to the WT (Fig. S9A-C). Both RT-qPCR and immunoblot analysis showed that *SlBRC2a* levels were elevated in *OE-SlBRC2a* lines, whereas *Wo* expression was largely unaffected (Fig. S9D&E). In contrast, all previously identified Wo downstream genes exhibited considerable down-regulation in *OE-SlBRC2a* lines (Fig. S9F-H), suggesting that SlBRC2a may affect Wo transcriptional activity.

6. SlBRC2a promotes cell expansion via suppressing *CKX* gene in basal cells

Our observation indicates that cell expansion occurs after extensive cell division in tomato trichomes (Fig. 1I-J). To understand the cell expansion alteration in *cr-slbrc2a* mutant, we extracted the trichomes from the WT and *cr-slbrc2a* mutant stem cells for RNA-seq analysis. We found that several *CKX* (*cytokinin oxidase/hydrogenase*) genes including *CKX1* and *CKX3*, genes involved in cytokinin degradation (Schmülling et al., 2003; Werner et al., 2003), were highly expressed in the *cr-slbrc2a* mutant (Suppl. data set S2, Fig. 8A). Consistent with this finding, a

previous report showed that the SlBRC2a-like homolog BRC1 inhibited tomato lateral bud formation via regulating the expression of the *CKX7* (Dong et al., 2023). Therefore, it is possible that cytokinin accumulation is also involved in SlBRC2a mediated cell expansion in basal cells. To this end, we examined the cytokinin content in the trichomes on the stem of WT and *cr-slbrc2a* mutants. The measurement showed a marked reduction in cytokinin content in the trichomes of the *SlBRC2a* mutant (Fig. 8B).

To further validate this *in vivo*, we generated transgenic tomato lines expressing the cytokinin marker, *TCS:VENUS-NLS*. VENUS fluorescence showed a similar pattern to that of *proSlBRC2a: SlBRC2a-GFP* in long DT (Fig. 8C and Fig. 4C). Next, we specifically expressed the *CKX1* gene in trichomes with the promoter of *Wo* or *SlBRC2a* (*proWo:CKX1-GFP* and *proSlBRC2a:CKX1-GFP*) (Fig. S9I). In both lines, the trichome cells became significantly smaller with a markedly reduced nuclear size (Fig. 8D-G). These results suggest that SlBRC2a promotes the endoreduplication and cell expansion in basal cells by negatively regulating the expression of the cytokinin degradation gene *CKX*.

Discussion

Woolly regulates multicellular trichome development in a dose-dependent manner

Tomato trichomes, which protrude from the surface, represent an excellent system for studying plant organogenesis. In this multicellular organ, organogenesis all starts from the trans-differentiation of a single cell, which then experiences cell fate determination, followed by morphogenesis including spatially organized cell division and cell differentiation, eventually resulting in seven types of trichomes with distinct morphology and functions. Once the trichome initial cells are formed, the trichome cell files first enter the division stage, and then maintain the polarized distribution of cell division in apical cells and cell expansion in basal cells. Interestingly, a single master regulator called Woolly (Wo) is involved in the regulation of all these distinct processes.

One strategy that Wo employs is concentration dependent mechanisms by which varying Wo concentrations bias the different trichome fates. In this study, we have shown that the Wo gradient is essential for establishing the polarized developmental pattern of tomato trichomes. High Wo levels in apical cells confer high mitotic capacity, whereas lower Wo concentration in basal cells

favors the transition from cell division to endoreduplication and cell expansion. In addition to Wo concentration, *SlBRC2a*, a downstream gene of Wo, interacts with Wo to inhibit Wo transcriptional activity, promoting the transition of basal cells from cell division to cell expansion (Fig. 9). Our results indicate that Wo gradients function not only spatially, but also at different temporal stages, to direct both fate determination and organ morphogenesis in the L1 epidermis of plants. This versatility of Wo can also be reflected by the fact that Wo can physically interact with most of the reported regulators of tomato trichome development including Hair (H), MYC1, Solanum lycopersicum WUSCHEL-related homeobox 3b (SlWox3b), and MX1 (Chang et al., 2018; Hua et al., 2020; Wu et al., 2023b). In addition, negative regulators of tomato trichomes, including MTR and JAZ, have also been shown to target the Wo protein (Yang et al., 2011; Hua et al., 2020; Wu et al., 2020; Wu et al., 2023b). Together, these lines of evidence support that Wo is likely to act as a versatile master regulator during tomato trichome development.

Dosage-dependent mechanism is employed by multiple HD Zip proteins

In Arabidopsis, Wo homolog, AtML1 acts in a similar way. At high concentrations, AtML1 promotes the epidermal cells of the sepal to form giant cells. In contrast, low AtML1 levels favor active mitosis, resulting in divided small cells (Meyer et al., 2017). It is not yet known whether there are thresholds for different protein concentrations that regulate different developmental processes. Interestingly, this concentration-dependent activity appears to be cell-type specific. Cell division is promoted by low levels of AtML1 in sepal epidermal cells, but by high levels of Wo in tomato trichomes. One possible reason for such divergence is that different perceiving cells have distinct downstream genes. Wo function relies on its downstream genes as simultaneous mutations of key Wo downstream regulators *SlWox3b*, *MX1* and *LEAFLESS* (*LFS*) gave rise to a single cell trichome without any division (Wu et al., 2023b), which looks similar to the giant cells in the sepal. It has been reported that the endoreduplication in both Arabidopsis trichomes and sepal giant cells is controlled by the regulation of cell cycle genes, including *SIAMESE* (Walker et al., 2000; Schnittger et al., 2002; Churchman et al., 2006; Roeder et al., 2012; Robinson et al., 2018; Wang et al., 2020). It is therefore interesting to further investigate whether the critical regulators uncovered in this study, SlBRC2a, SlWox3b and MX1, affect the balance between cell division and endoreduplication in multicellular trichomes via regulation of these cell cycle genes.

Wo protein gradient may be maintained by multiple factors

Despite both forming gradient, Wo is actually different from morphogen. The gradient of Wo is generated by a series of positive and negative feedback loops. During the trichome initiation, the dramatic increase of Wo concentration in initial cells could partially result from the self-activation (Wu et al., 2023b). In trichome morphogenesis, Wo level in type I and II trichomes is way higher than that in type IV and V, even all of them belong to DT (Fig. 2A). Therefore, in addition to self-activation, Wo could have other ways to enhance its expression.

Our previous results showed that knockout of *Hair* (*H*) and *Hair-Like* (*HL)*, two C2H2 transcription factors downstream of Wo, caused the disappearance of type I and II trichomes (Chang et al., 2018; Chun et al., 2021; Li et al., 2021; Zheng et al., 2021; Hua et al., 2022). We speculate that the function of H and HL may be associated with the high level of Wo in type I and II trichomes. Besides positive feedback loops, Wo also has multiple negative feedback regulations. During the trichome initiation, Wo protein levels are subject to the suppression by E3-ligase like proteins called MTRs (Wu et al., 2020; Wu et al., 2023b). This negative feedback loop maintains Wo concentration fluctuate within a certain spectrum. In this study, we provide alternative way to repress Wo activity. In basal cells of trichomes, SlBRC2a physically interacts with Wo, restricting Wo transcriptional activity, which not only impairs Wo self-activation, but inhibits Wo activation of several key downstream genes. The resulting combinatorial effect is the quick reduction of Wo level and its activity in promoting cell division. Interestingly, *MTRs* are also expressed in the dividing apical cells, which is likely to prevent the over division of apical cells (Fig. 2B-D). It still remains to be shown whether the expression of *MTR* genes in apical cells prevents the activation of *SlBRC2a*.

According to previous studies, CYC/TB1 TCP proteins are mostly involved in the regulation of processes such as branching and floral organ morphogenesis (Aguilar-Martínez et al., 2007; Broholm et al., 2008; Zhao et al., 2018; Shang et al., 2020). Here we find no phenotype of tomato lateral buds when BRC2-like gene *SlBRC2a* is knocked out (Fig. S4C). In addition, *SlBRC2a* is specifically expressed in the basal cells of tomato trichomes (Fig. 4B-C), and seems to promote cytokinin biosynthesis via repressing *CKX1/3*. In Arabidopsis roots, cytokinin was also reported to promote the transition to cell expansion of root cells (Ioio et al., 2008). During tomato lateral bud development, BRC1 can directly bind to the promoter of *CKX7* and activate its expression (Dong et al., 2023), suggesting SlBRC2a and BRC1 have distinct roles. Similar to the antagonism

between cytokinin and auxin in promoting cell expansion of the root cells, CsBRC1 has been shown to suppress the expression of *CsPIN3* during the lateral shoot formation in cucumber (*Cucumis sativus*) (Shen et al., 2019). It needs further study to know whether SlBRC2a affects cell expansion of tomato trichomes in additional pathways (Fig. 9).

Our results indicate that the homeostasis of Wo is a key for the regulation of different aspects of tomato trichomes. Studies of other homeobox domain proteins showed similar results. The stem cells in shoot apical meristem and root apical meristem are regulated by two homeobox domain genes, *WUSCHEL* (*WUS*) and *WUSCHEL-related homeobox 5* (*WOX5*). The expression of both genes is confined by CLV3 and IAA17 (Brand et al., 2000; Tian et al., 2014; Wu et al., 2023a). The activity of the HD-Zip III protein REV, a regulator of leaf polarity and vascular bundle development, is inhibited by a negative feedback loop of the ZPR protein (Wenkel et al., 2007). It seems to be a general principle for the regulation of HD gene function. The feedback loops, particularly the negative feedback can function as an activity brake or confine the function in a spatially restricted region. Interestingly, the repression of Wo by SlBRC2a may be a conserved mechanism, as TEOSINTE BRANCHED1, CYCLOIDEA, and PCF17 (MdTCP17) was recently reported to interact with WUSCHEL-related homeobox11 (MdWOX11) to reduce the expression of the MdWOX11 downstream gene *LATERAL ORGAN BOUNDARIES DOMAIN29* (*MdLBD29*) during adventitious root primordium formation in apple (*Malus domestica*) (Mao et al., 2023). HD-Zip IV genes are unique to plants, and many of them have been found to play roles in L1 epidermal layer (Abe et al., 2001; Rombola-Caldentey et al., 2014; Sun et al., 2020). It still needs further work to dissect how the spatiotemporal fine-tune of HD-Zip IV gene function to drive the epidermal differentiation.

Multicellular trichomes have been extensively studied in different species, such as Qinghao (*Artemisia annua*), tobacco (*Nicotiana tabacum*), cucumber (*Cucumis sativus*) and mint (*Mentha arvensis*), due to their high pharmacological values (Schilmiller et al., 2008; Huchelmann et al., 2017; Tissier, 2018). Interestingly, several lines of evidence support the conserved role of HD-Zip IV genes in the regulation of the trichome initiation in these species (Pan et al., 2015; Cui et al., 2016; Wang et al., 2016; Yan et al., 2016; Yan et al., 2018; Du et al., 2020; Wu et al., 2020; Qi et al., 2022). It is not yet known whether these HD-Zip IV genes are responsible for the diversification of multi-cellular trichomes in different species. Our studies indicate that the

regulation of HD-Zip IV genes may be multi-layered, both at the transcriptional and protein levels. In addition, recent studies showed that the stability of HD-Zip IV proteins in the L1 layer is associated with the lipid metabolism and signaling (Izabela et al., 2021; Nagata et al., 2021; Schrick et al., 2023).Therefore, the regulatory network of HD-Zip IV protein concentration in the L1 layer is quite complex, and further investigation of HD-Zip IV regulation may lead to a better understanding of the differentiation of the L1 layer and the epidermis.

Materials and Methods

Plant growth conditions and materials

Tomato (*Solanum lycopersicum*) Micro-Tom was used as the wild-type background material in this study. Transgenic material and WT seeds were germinated and planted in 9 × 9 × 9 cm pots, and plants were grown in a 1:1 mixture of substrate soil and vermiculite with Hoagland nutrient solution. All tomato plant materials were grown in greenhouse conditions (28°C under 16-h light and 26°C at 8-h dark, with 12,000 Lux illumination intensity from emitting diode light source and 70% relative humidity). *Nicotiana benthamiana* for LUC experiments were grown in 1/2 MS medium in a constant temperature incubator (Hi-Point F-1300, 16-h light/8-h dark at 26°C, with 12,000 Lux illumination intensity and 70% relative humidity). *Arabidopsis thaliana* materials were grown in greenhouse conditions (22°C under 16-h light and 18°C at 8-h dark, with 12,000 Lux illumination intensity from emitting diode light source and 55% relative humidity).

Phylogenetic analyses

CIN and CYC/TB1 TCP protein sequences were downloaded from the Sol Genomics Network (https://solgenomics.net/, SL4.0) (Fernandez-Pozo et al., 2015) and TAIR (https://www.arabidopsis.org/). Details of these proteins are provided in Supplemental Data Set S3. Sequences were aligned using MUSCLE method in the MEGA 7 software (Kumar et al., 2016). The aligned sequences were used to construct phylogenetic trees in MEGA 7 by using the maximum-likelihood (ML) method. The robustness of the ML tree topology was assessed with 1,000 bootstrap replicates. The tree was drawn to scale, with branch lengths measured in the number of substitutions per site.

Vector construction and tomato transformation

The promoter sequences and full-length CDS sequences used in this study were obtained from the Solanaceae Genomics Network database (https://solgenomics.net/) (Fernandez-Pozo et al., 2015). DNA fragments were amplified using KOD One^{TM} PCR Master Mix (KMM-101). Fragments were ligated to the vector using the Clone Express II One Step Cloning Kit (Vazyme Biotech, C112-01/02). CRISPR/Cas9-mediated knockout targeting of *SlBRC2a* was performed using CRISPR-PLANT (https://www.genome.arizona.edu/crispr/) (Liu et al., 2017) for screening. *OE-SlBRC2a* vectors were created by inserting the CDS sequence of *SlBRC2a* into the *pHELLSGATE8* vector with *CaMV 35S* as the promoter between EcoR I restriction site. *MX1* promoter driven Wo^{v}-GFP fusion protein expression vector (*proMX1:Wo^{v}-GFP*) and *Wo* promoter, *SlBRC2a* promoter driven CKX1-GFP expression vectors (*proWo:CKX1-GFP*, *proSlBRC2a:CKX1-GFP*) were constructed by sequentially ligating promoter sequences and CDS sequences into the *pHELLSGATE8* vector with EcoR I restriction site. *proSlBRC2a:GFP-GUS* reporter vector was constructed by ligating the *SlBRC2a* promoter sequence into the *pHELLSGATE8* vector fused with the GFP-GUS protein between Sac I and Xba I restriction sites. The constructed plasmids were transformed into *Agrobacterium tumifaciens* C58 cells and infiltrated with tomato cotyledon tissues. The infested cuttings were continued to co-culture for 2 d and then transferred to screening medium, followed by 1-2 successions after sprouting, and eventually rooting culture to obtain transgenic tomato plants. Transgenic plant DNA was extracted using the CTAB method to detect knockout plants. GUS staining and GFP fluorescence (as same as the Phenotypic observation and quantification section) observation were used to detect transgenic plants with marker genes. Protein level in transgenic plants was detected using immunoblot. *cr-slbrc2a* x *pro35S:H2B-GFP*, *cr-slbrc2a* x *proWo:Wo-GFP*, *cr-slbrc2a* x *proWo:Wo^{P635R}-GFP*, *cr-slbrc2a* x *cr-mx*1, *cr-slbrc2a* x *mtr1 mtr2* were obtained by conventional crossing. All used primers are listed in Suppl. Data Set S4.

Phenotypic observation and quantification

Cell division and Wo level in the trichomes of *pro35S:H2B-GFP*, *proWo:Wo-GFP* and *cr-slbrc2a x proWo:Wo-GFP* seedlings were observed using a Zeiss LSM 880 confocal microscope with dual-channel setting of GFP and PI(GFP 488-nm excitation/493-548 nm with PMT detector gain is

700, PI 561-nm excitation/570–645 nm with PMT detector gain is 650). The cell wall of tomato trichomes sometimes prevents the effective DAPI (4,6-diamidino-2-phenylindole, Sigma, D9542) staining, so we also used H2B-GFP as an indicator of the chromatin abundance (Kanda et al., 1998). According to the previously established technique, the nuclear area can be quantified as a proxy for nuclear volume (Walker et al., 2000). Nuclei from stem trichomes of *pro35S:H2B-GFP* and *cr-slbrc2a x pro35S:H2B-GFP* plants (5-week-old) were used for nuclear size calculation. In addition, we modified the DAPI staining to overcome the cell wall barrier, the details were as follows:1μg/ml DAPI + 0.1% tritonX-100(v/v), staining for 12h. Nuclear area of stomatal cells was used as a control (2C) (Melaragno et al., 1993). PI staining (0.01μg/ml) was used for microscopy preparation of GFP fluorescence imaging, and ddH_2O for DAPI fluorescence imaging. All the images of trichome were obtained with maximum intensity projection of Z-stacks. Nuclei area and fluorescence intensity were quantified using ImageJ and ZEN software.

Mature trichomes on the stem of WT and *cr-slbrc2a* plants about 5-week-old were counted for cell number under a DIC microscope. GUS staining of *proSlBRC2a:GFP-GUS* seedlings and young leaves was observed using a LEICA M205 FA microscope. The phenotype of trichome was also observed using a Hitachi TM3030Plus scanning electron microscope (15KV-SE), and we use pseudo-color to highlight a trichomes or single cells by Adobe Photoshop.

Flow cytometry analysis

For flow cytometry, long trichomes on the stem of the 5-week-old tomato plants were pulled out individually with sharp forceps under a dissecting microscope. The extracted long trichomes usually carry a small piece of detached epidermal tissue at the base. Trichomes were collected from 5 wild-type plants and 10 *cr-slbrc2a* plants. For the comparison, the 4th to 5th Arabidopsis leaves were collected from the 3-week-old plants. All collected tissues were chopped with a razor blade in 2 ml nuclei isolation buffer (NIB) (Tian et al., 2020): 10 mM MES-KOH (pH 5.4), 10 mM NaCl, 10 mM KCl, 2.5 mM ethylene diamine tetra-acetic acid (EDTA), 250 mM sucrose, 0.1 mM spermine, 0.5 mM spermidine, 1 mM dithiothreitol (DTT). The nuclei were filtered through a 70 μm mesh and stained with 50 μg/ml PI (propidium iodide). Nuclear DNA content was analyzed with an Attune NxT flow cytometer (Invitrogen), with a voltage of FFC (180), SSC (380) and BL2 (280). Data were collected for approximately 15,000 nuclei per sample and presented on a linear axis.

RNA Extraction and reverse transcription quantitative PCR (RT-qPCR)

Mature trichomes on the stem of 5-week-old tomato plants were taken for RNA extraction. Stem tissues were snap frozen in liquid nitrogen, and then the trichomes were scraped with a spoon onto a nylon cloth. The collected trichomes were ground into a powder for RNA extraction. Young leaf tissue was obtained from 2-week-old tomato seedlings. Total RNA extraction was performed using Promega Eastep® Super Total RNA Extraction Kit (LS1040). Promega GoScript Reverse Transcriptase (GoScript™ A5003) was used to synthesize cDNA. RT-qPCR was performed using AceQ qPCR SYBR Green Master Mix (Vazyme Biotech, Q121-02) reaction in a CFX384 Real-Time system (BIO-RAD) with *SlActin* 2 as the internal reference gene. More than three independent biological replicates were conducted for each sample and three technical replicates were performed for each biological replicate. The relative expression was calculated by the ΔΔct method. Primers are listed in Suppl. data set S4.

RNA-sequencing

RNA extraction was performed as above, with three biological replicates set up for each sequenced material. RNA-seq library construction, sequencing and analysis were performed as described in previous literature (Hua et al., 2020). Standard RNA sequencing libraries were generated using the TruSeq Stranded Total RNA Library Prep Kit (Illumina) and sequenced by the Illumina sequencing system on the Hiseq 2500 platform (Illumina, Novogene). Significance was assessed using a threshold of $|\log_2$ fold change$|>1$ and False discovery rate (FDR) <0.001 corrected by multiple significance tests.

Yeast two-hybrid assay

Protein-protein binding was verified using the Yeast two-hybrid system (Clontech). The full-length CDS sequence encoding the target protein was inserted to *pGBKT7* and *pGADT7* as bait and prey, respectively. Primers are listed in Suppl. Data Set S4. The two plasmids were co-transferred into AH109 yeast (*Saccharomyces cerevisiae*) cells by lithium acetate transformation method and coated on SD/-Trp/-Leu (DDO, double drop out medium) medium for screening. The yeast were collected in an appropriate amount of sterile ddH_2O after 3 d of growth in an incubator at 30°C, and then diluted according to OD600 (1, 0.1, 0.01), and 10 μl of each yeast was spotted on SD/-Trp/-Leu (DDO) and SD/-Trp/-Leu/-His/-Ade (QDO, quadruple drop out medium) media. The growth of the yeast was observed after 3-5 d in an incubator at 30°C. The interaction was

determined if yeast grows well at all concentration gradients in SD/-Trp/-Leu/-His/-Ade (QDO) medium.

Yeast one-hybrid assay

Binding of the protein to the promoter was verified using a yeast single hybridization system. The full-length CDS sequence encoding the target protein was inserted to the pJG4-5 vector as a prey, and the target gene promoter sequence was ligated to the pLacZi vector as a bait. Primers are listed in Suppl. Data Set S4. Both vectors were co-transformed into EGY48 yeast cells by lithium acetate transformation method and coated on SD/-Trp/-Ura medium for screening. After growing for 3 d in an incubator at 30°C, the yeast cells were collected in an appropriate amount of sterile ddH_2O. OD600 was adjusted to about 1, and 5 μl of the yeast solution was spotted on SD/-Trp/-Ura/+X-gal medium and incubated at 30°C and protected from light for 3-5 days. The interaction is determined if blue color appears.

GUS Staining

The leaf tissues were completely immersed in GUS staining solution: 10 mM EDTA disodium salt, 100 mM NaH_2PO_4, 0.5 mM $K_4Fe(CN)_6$, 0.5 mM $K_3Fe(CN)_6$, 0.1% Triton-X100 (v/v), 0.5 mg/ml X-gluc (Golden Biotechnology, G1281C1), pH=7.0. After 10-12 hours at 37°C, the samples were decolorized in ethanol : acetic acid (4 : 1) solution for 3 hours and finally stored in 75% ethanol for observation.

Protoplast isolation and Luciferase (LUC) Assay

The plasmids used in this study for LUC and Co-IP experiments were extracted by the PEG8000 precipitation method. Young *Nicotiana benthamiana* and *pro35S:NbMTR1-GFP* leaves were used for protoplast preparation, and the protoplasts were extracted by reference to (Yoo et al., 2007). The promoter sequence and the full-length coding sequence were inserted into the p*Green-0800-II* vector (reporter) and the *pXSN-FLAG* vector (effector), respectively. Primers are listed in Suppl. Data Set S4. Effectors and reporters were co-transferred into protoplasts in a 1:5 ratio according to the previously described method (Wu et al., 2020). Protoplasts were incubated at room temperature for 12 hours and then harvested for LUC activity analysis. LUC activity was measured using a Dual-Luciferase® reporter analysis system (Promega, E1910). Luminescence of LUC and REN was detected with a CYTATION5 image reader (BioTek). LUC values were normalized to REN values. Three biological replicates were measured for each combination.

Co-Immunoprecipitation and immunoblot

To express fusion proteins for Co-IP, the CDS of *SlBRC2a* and *Wo* genes were amplified by PCR and inserted into the vector *pXSN-FLAG* or *pXSN-GFP*. Primers are listed in Suppl. Data Set S4. The fusion constructs were expressed in the *N. benthamiana* protoplast. After incubation 12h, protoplast cells were harvested and lysed with IP lysis buffer (50mM HEPES pH 7.5, 50mM NaCl, 10mM EDTA, 0.2% Triton X-100(v/v), 10% Glycerol(v/v), 2mM DTT, 1 x protease inhibitor (Roche), 1 x PMSF (Solarbio, P0100-1), 80μM MG132 (MCE, HY-13259) on ice for 15 min, followed by centrifugation for 10 min at 13520 g at 4°C. The Wo-GFP fusion protein was incubated with GFP-Nanoab-Magnetic Beads (BEIJING LABLEAD BIOTECHNOLOGY CO. LTD., GNM-50-2000) for 2 h at 4°C. After four washes with PBS, the Co-IP products were collected and analyzed by immunoblot. The samples were resolved by SDS-PAGE and immuno-blotted using anti-GFP antibody (TransGen Biotech Co., Ltd, HT801-02, 1:1000 dilution), anti-Flag antibody (BEIJING LABLEAD BIOTECHNOLOGY CO.,LTD., F1005, 1:2000 dilution), anti-HRP Secondary antibodies (Sigma, A5278, 1:3000~1:5000 dilution).

Protein purification and in vitro pull-down assay

For protein purification, we cloned the full-length coding sequence of *SlBRC2a* into vector pMAL-c5X. The fusion proteins were expressed in the *Escherichia coli* strain BL21 (DE3) induced by 250μm/L isopropyl-b-D-thiogalactoside (IPTG) and purified using MBP beads (NEB, E8021S). Wo-GFP protein was purified from the *proWo:Wo-GFP* transgenic plants. The purified recombinant proteins were incubated with GFP magic beads for the pull-down assays in IP lysis buffer at 4°C for 1 h. The samples were washed five times with the washing buffer (50mM HEPES pH 7.5, 150mM NaCl, 10mM EDTA, 0.1% Triton X-100(v/v), 10% Glycerol(v/v), 1 x PMSF) and then boiled for 10 minutes in 1 x SDS loading buffer. The samples were resolved by SDS-PAGE and immuno-blotted using anti-GFP antibody (TransGen Biotech Co., Ltd, HT801-02, 1:1000 dilution), anti-MBP antibody (NEB, E8032S, 1:10000 dilution), and anti-HRP Secondary antibodies (Sigma, A5278, 1:3000~1:5000 dilution).

Bimolecular fluorescence complementation (BiFC)

CDSs of *Wo* and *SlBRC2a* genes were amplified and fused to N-terminal half of YFP (2YN) or C-terminal half of YFP (2YC). Primers are listed in Suppl. data set S4. The recombinant

constructs were transformed into *A. tumefaciens* GV3101. Leaves of 5-week-old *N. benthamiana* were infiltrated with the transformed *A. tumefaciens* cells. The transformed leaves were imaged with a confocal microscope (Zeiss, Dresden, Germany) after 48-72 h of incubation.

Measurement of cytokinin concentration in trichome

Mature trichomes on the stem of 5-week-old tomato plants were taken for detection of cytokinin content, and the sampling method was the same as the RNA extraction described above. Ethyl acetate was added to the powder sample (sample mass ratio was 1/10), and in low temperature ultrasonic crusher for 20 minutes, the supernatant was taken for concentration after centrifuge. 200 μl 70% methanol was added to redissolve, filter the liquid with 0.22 μm PVDF membrane after centrifuge, which could be used to detect the content of cytokinin. The above extraction steps were all carried out at 4°C. The hormone standard (trans-Zeatin, catalog number: 001030) used for detection was from OlChemIm, and the detection was carried out using a UPLC-XEVO TQ-S MS triple quadrupole mass spectrometer (Waters, Milford, MA, USA) equipped with an ACQUITY UPLC BEH C18 column (2.1 × 100 mm, 1.7 μm). A calibration curve made from a hormone standard was used to calculate hormone content.

Quantification and statistical analysis

The quantification was statistically analyzed by GraphPad. P-values were calculated by two-tailed unpaired Student's t-test. The t test results are listed in Supplemental Data Set S5. The definition of significance is described in each figure legend. All data were represented as mean ± SD.

Accession Numbers

Sequence data from this article can be found in the Sol genomics databases under the following accession numbers: *Woolly*, Solyc02g080260; *SlBRC2a*, Solyc04g006980, *MTR1*, Solyc10g083140; *MTR2*, Solyc06g073990; *MX1*, Solyc01g010910; *CKX1*, Solyc10g079870; *CKX3*, Solyc12g008900; *ACTIN2*, Solyc11g005330. RNA-seq raw data have been deposited in National Genomics Data Center (NGDC) under GSA-plant (project number: PRJCA021910).

Funding information

This work is supported by the grant from the National Natural Science Foundation of China (32370354).

Acknowledgments

We thank Ms. RuiMei Wu and Dr. XiaoMin Yu for the help in cytokinin measurement and Dr. Quan Wang for *TCS:VENUS-NLS* seeds. We also to thank Ms. Shan Xu and Ms. XiaoDan Ma for their help in the flow cytometry analysis.

Author Contributions

M.L. Wu and S. Wu conceived and designed the experiments; M.L. Wu, X.X. Bian, S.R. Hu, B.B. Huang, J.Y. Shen, Y.D. Du, Y.L. Wang, and M.Y. Xu. performed most of the experiments and analyzed the data; X.X. Bian, S.R. Hu, B.B. Huang, J.Y. Shen, and M.N. Yang performed tomato

stable transformation; H.M. Xu analyzed RNA-seq data; M.L. Wu and S. Wu wrote the article.

Competing Interest Statement: The authors declare no competing interest.

References

Abe, M., Takahashi, T., and Komeda, Y. (2001). Identification of a cis-regulatory element for L1 layer-specific gene expression, which is targeted by an L1-specific homeodomain protein. The Plant Journal **26,** 487-494.

Aguilar-Martínez, J.A., Poza-Carrión, C.s., and Cubas, P. (2007). Arabidopsis BRANCHED1 Acts as an Integrator of Branching Signals within Axillary Buds. The Plant cell **19,** 458-472.

Anirban, A. (2022). 70 years of Turing patterns. Nature Reviews Physics **4,** 432-432.

Ariel, F.D., Manavella, P.A., Dezar, C.A., and Chan, R.L. (2007). The true story of the HD-Zip family. Trends in plant science **12,** 419-426.

Brand, U., Fletcher, J.C., Hobe, M., Meyerowitz, E.M., and Simon, R. (2000). Dependence of Stem Cell Fate in Arabidopsis on a Feedback Loop Regulated by CLV3 Activity. Science **289,** 617-619.

Broholm, S.K., Tähtiharju, S., Laitinen, R.A.E., Albert, V.A., Teeri, T.H., and Elomaa, P. (2008). A TCP domain transcription factor controls flower type specification along the radial axis of the Gerbera (Asteraceae) inflorescence. Proceedings of the National Academy of Sciences **105,** 9117-9122.

Chang, J., Yang, J., Wang, J., and Wu, S. (2021). Comprehensive observation of trichome development in Micro-tom tomato. Vegetable Research **1,** 1-9.

Chang, J., Yu, T., Yang, Q., Li, C., Xiong, C., Gao, S., Xie, Q., Zheng, F., Li, H., Tian, Z., Yang, C., and Ye, Z. (2018). Hair, encoding a single C2H2 zinc-finger protein, regulates multicellular trichome formation in tomato. The Plant journal : for cell and molecular biology **96,** 90-102.

Chun, J.-I., Kim, S.-M., Kim, H., Cho, J.-Y., Kwon, H.-W., Kim, J.-I., Seo, J.-K., Jung, C., and Kang, J.-H. (2021). SlHair2 Regulates the Initiation and Elongation of Type I Trichomes on Tomato Leaves and Stems. Plant and Cell Physiology **62,** 1446-1459.

Churchman, M.L., Brown, M.L., Kato, N., Kirik, V., Hu¨lskamp, M., Inzé, D., De Veylder, L., Walker, J.D., Zheng, Z., Oppenheimer, D.G., Gwin, T., Churchman, J., and Larkin, J.C. (2006). SIAMESE, a Plant-Specific Cell Cycle Regulator, Controls Endoreplication Onset in Arabidopsis thaliana. The Plant cell **18,** 3145-3157.

Cui, J.-Y., Miao, H., Ding, L.-H., Wehner, T.C., Liu, P.-N., Wang, Y., Zhang, S.-P., and Gu, X.-F. (2016). A New Glabrous Gene (csgl3) Identified in Trichome Development in Cucumber (Cucumis sativus L.). PloS one **11,** e0148422.

Deeks, M.J., Kaloriti, D., Davies, B., Malhó, R., and Hussey, P.J. (2004). Arabidopsis NAP1 Is Essential for Arp2/3-Dependent Trichome Morphogenesis. Current Biology **14,** 1410-1414.

Di Cristina, M., Sessa, G., Dolan, L., Linstead, P., Baima, S., Ruberti, I., and Morelli, G. (1996). The Arabidopsis Athb-10 (GLABRA2) is an HD-Zip protein required for regulation of root hair development. The Plant Journal **10,** 393-402.

Dong, H., Wang, J., Song, X., Hu, C., Zhu, C., Sun, T., Zhou, Z., Hu, Z., Xia, X., Zhou, J., Shi, K., Zhou, Y., Foyer, C.H., and Yu, J. (2023). HY5 functions as a systemic signal by integrating BRC1-dependent hormone signaling in tomato bud outgrowth. Proceedings of the National Academy of Sciences **120,** e2301879120.

Donnelly, P.M., Bonetta, D., Tsukaya, H., Dengler, R.E., and Dengler, N.G. (1999). Cell Cycling and Cell Enlargement in Developing Leaves of Arabidopsis. Developmental Biology **215,** 407-419.

Du, H., Wang, G., Pan, J., Chen, Y., Xiao, T., Zhang, L., Zhang, K., Wen, H., Xiong, L., Yu, Y., He, H., Pan, J., and Cai, R. (2020). The HD-ZIP IV transcription factor Tril regulates fruit spine density through gene dosage effects in cucumber. Journal of experimental botany **71,** 6297-6310.

Fernandez-Pozo, N., Menda, N., Edwards, J.D., Saha, S., Tecle, I.Y., Strickler, S.R., Bombarely, A., Fisher-York, T., Pujar, A., Foerster, H., Yan, A., and Mueller, L.A. (2015). The Sol Genomics Network (SGN)—from genotype to phenotype to breeding. Nucleic acids research **43,** D1036-D1041.

Gehring, W.J., Affolter, M., and Bürglin, T. (1994). HOMEODOMAIN PROTEINS. Annual Review of Biochemistry **63,** 487-526.

Glas, J.J., Schimmel, B.C., Alba, J.M., Escobar-Bravo, R., Schuurink, R.C., and Kant, M.R. (2012). Plant glandular trichomes as targets for breeding or engineering of resistance to herbivores. International journal of molecular sciences **13,** 17077-17103.

Grammatopoulos, G.A., Bell, E., Toole, L., Lumsden, A., and Tucker, A.S. (2000). Homeotic transformation of branchial arch identity after Hoxa2 overexpression. Development **127,** 5355-5365.

Hong, L., Rusnak, B., Ko, C.S., Xu, S., He, X., Qiu, D., Kang, S.E., Pruneda-Paz, J.L., and Roeder, A.H.K. (2023). Enhancer activation via TCP and HD-ZIP and repression by Dof transcription factors mediate giant cell-specific expression. The Plant cell **35,** 2349-2368.

Hua, B., Chang, J., Wu, M., Xu, Z., Zhang, F., Yang, M., Xu, H., Wang, L.-J., Chen, X.-Y., and Wu, S. (2020). Mediation of JA signalling in glandular trichomes by thewoolly/SlMYC1regulatory module improves pest resistance in tomato. Plant biotechnology journal **19,** 375-393.

Hua, B., Chang, J., Han, X., Xu, Z., Hu, S., Li, S., Wang, R., Yang, L., Yang, M., Wu, S., Shen, J., Yu, X., and Wu, S. (2022). H and HL synergistically regulate jasmonate-triggered trichome formation in tomato. Horticulture Research **9,** uhab080.

Huchelmann, A., Boutry, M., and Hachez, C. (2017). Plant Glandular Trichomes: Natural Cell Factories of High Biotechnological Interest. Plant physiology **175,** 6-22.

Hülskamp, M. (2004). Plant trichomes: a model for cell differentiation. Nature Reviews Molecular Cell Biology **5,** 471-480.

Ioio, R.D., Nakamura, K., Moubayidin, L., Perilli, S., Taniguchi, M., Morita, M.T., Aoyama, T., Costantino, P., and Sabatini, S. (2008). A Genetic Framework for the Control of Cell Division and Differentiation in the Root Meristem. Science **322,** 1380-1384.

Izabela, W., Thiya, M., Patrick, K.-B., Xueyun, H., Aashima, K., Graham, L.M., Kyle, A.T., Seth, T.P., Jagoda, S., Anja, T., Dirk, K.H., Aleksandra, S., and Kathrin, S. (2021). Arabidopsis PROTODERMAL FACTOR2 binds lysophosphatidylcholines and transcriptionally regulates phospholipid metabolism. bioRxiv**,** 2021.2010.2020.465175.

Jegalian, B.G., and De Robertis, E.M. (1992). Homeotic transformations in the mouse induced by overexpression of a human Hox3.3 transgene. Cell **71,** 901-910.

Kanda, T., Sullivan, K.F., and Wahl, G.M. (1998). Histone-GFP fusion protein enables sensitive analysis of chromosome dynamics in living mammalian cells. Current Biology **8,** 377-385.

Kumar, S., Stecher, G., and Tamura, K. (2016). MEGA7: Molecular Evolutionary Genetics Analysis Version 7.0 for Bigger Datasets. Molecular biology and evolution **33,** 1870-1874.

Li, R., Wang, X., Zhang, S., Liu, X., Zhou, Z., Liu, Z., Wang, K., Tian, Y., Wang, H., Zhang, Y., and Cui, X. (2021). Two zinc-finger proteins control the initiation and elongation of long stalk trichomes in tomato. Journal of Genetics and Genomics **48,** 1057-1069.

Liu, H., Ding, Y., Zhou, Y., Jin, W., Xie, K., and Chen, L.L. (2017). CRISPR-P 2.0: An Improved CRISPR-Cas9 Tool for Genome Editing in Plants. Molecular plant **10,** 530-532.

Mao, J., Niu, C., Li, K., Fan, L., Liu, Z., Li, S., Ma, D., Tahir, M.M., Xing, L., Zhao, C., Ma, J., An, N., Han, M., Ren, X., and Zhang, D. (2023). Cytokinin-responsive MdTCP17 interacts with MdWOX11 to repress adventitious root primordium formation in apple rootstocks. The Plant cell **35,** 1202-1221.

Martín-Trillo, M., and Cubas, P. (2010). TCP genes: a family snapshot ten years later. Trends in plant science **15,** 31-39.

Melaragno, J.E., Mehrotra, B., and Coleman, A.W. (1993). Relationship between Endopolyploidy and Cell Size in Epidermal Tissue of Arabidopsis. The Plant cell **5,** 1661-1668.

Meyer, H.M., Teles, J., Formosa-Jordan, P., Refahi, Y., San-Bento, R., Ingram, G., Jönsson, H., Locke, J.C., and Roeder, A.H. (2017). Fluctuations of the transcription factor ATML1 generate the pattern of giant cells in the Arabidopsis sepal. eLife **6,** e19131.

Nagata, K., Ishikawa, T., Kawai-Yamada, M., Takahashi, T., and Abe, M. (2021). Ceramides mediate positional signals in Arabidopsis thaliana protoderm differentiation. Development **148**.

Ohashi, Y., Oka, A., Ruberti, I., Morelli, G., and Aoyama, T. (2002). Entopically additive expression of GLABRA2 alters the frequency and spacing of trichome initiation. The Plant Journal **29,** 359-369.

Pan, Y., Bo, K., Cheng, Z., and Weng, Y. (2015). The loss-of-function GLABROUS 3 mutation in cucumber is due to LTR-retrotransposon insertion in a class IV HD-ZIP transcription factor gene CsGL3 that is epistatic over CsGL1. BMC plant biology **15,** 302.

Perrimon, N., Pitsouli, C., and Shilo, B.Z. (2012). Signaling mechanisms controlling cell fate and embryonic patterning. Cold Spring Harbor perspectives in biology **4,** a005975.

Peterson, K.M., Shyu, C., Burr, C.A., Horst, R.J., Kanaoka, M.M., Omae, M., Sato, Y., and Torii, K.U. (2013). Arabidopsis homeodomain-leucine zipper IV proteins promote stomatal development and ectopically induce stomata beyond the epidermis. Development **140,** 1924-1935.

Qi, X., Chen, Z., Yu, X., Li, L., Bai, Y., Fang, H., and Liang, C. (2022). Characterisation of the Mentha canadensis R2R3-MYB transcription factor gene McMIXTA and its involvement in peltate glandular trichome development. BMC plant biology **22,** 219.

Robinson, D.O., Coate, J.E., Singh, A., Hong, L., Bush, M., Doyle, J.J., and Roeder, A.H.K. (2018). Ploidy and Size at Multiple Scales in the Arabidopsis Sepal. The Plant cell **30,** 2308-2329.

Roeder, A.H.K., Cunha, A., Ohno, C.K., and Meyerowitz, E.M. (2012). Cell cycle regulates cell type in the Arabidopsis sepal. Development **139,** 4416-4427.

Rombola-Caldentey, B., Rueda-Romero, P., Iglesias-Fernandez, R., Carbonero, P., and Onate-Sanchez, L. (2014). Arabidopsis DELLA and two HD-ZIP transcription factors regulate GA signaling in the epidermis through the L1 box cis-element. The Plant cell **26,** 2905-2919.

Sagner, A., and Briscoe, J. (2017). Morphogen interpretation: concentration, time, competence, and signaling dynamics. WIREs Developmental Biology **6,** e271.

Schilmiller, A.L., Last, R.L., and Pichersky, E. (2008). Harnessing plant trichome biochemistry for the production of useful compounds. The Plant Journal **54,** 702-711.

Schmülling, T., Werner, T., Riefler, M., Krupková, E., and Bartrina y Manns, I. (2003). Structure and function of cytokinin oxidase/dehydrogenase genes of maize, rice, Arabidopsis and other species. Journal of Plant Research **116,** 241-252.

Schnittger, A., Schöbinger, U., Stierhof, Y.-D., and Hülskamp, M. (2002). Ectopic B-Type Cyclin Expression Induces Mitotic Cycles in Endoreduplicating Arabidopsis Trichomes. Current Biology

12, 415-420.

Schrick, K., Ahmad, B., and Nguyen, H.V. (2023). HD-Zip IV transcription factors: Drivers of epidermal cell fate integrate metabolic signals. Current opinion in plant biology **75,** 102417.

Shang, Y., Yuan, L., Di, Z., Jia, Y., Zhang, Z., Li, S., Xing, L., Qi, Z., Wang, X., Zhu, J., Hua, W., Wu, X., Zhu, M., Li, G., and Li, C. (2020). A CYC/TB1-type TCP transcription factor controls spikelet meristem identity in barley. Journal of experimental botany **71,** 7118-7131.

Shen, J., Zhang, Y., Ge, D., Wang, Z., Song, W., Gu, R., Che, G., Cheng, Z., Liu, R., and Zhang, X. (2019). CsBRC1 inhibits axillary bud outgrowth by directly repressing the auxin efflux carrier CsPIN3 in cucumber. Proceedings of the National Academy of Sciences **116,** 17105-17114.

Simmons, A.T., and Gurr, a.G.M. (2005). Trichomes of Lycopersicon species and their hybrids: effects on pests and natural enemies. Agricultural and Forest Entomology **7,** 265-276.

Sun, J., Cui, X., Teng, S., Kunnong, Z., Wang, Y., Chen, Z., Sun, X., Wu, J., Ai, P., Quick, W.P., Lu, T., and Zhang, Z. (2020). HD-ZIP IV gene Roc8 regulates the size of bulliform cells and lignin content in rice. Plant biotechnology journal **18,** 2559-2572.

Szymanski, D.B., Marks, M.D., and Wick, S.M. (1999). Organized F-Actin Is Essential for Normal Trichome Morphogenesis in Arabidopsis. The Plant cell **11,** 2331-2347.

Szymanski, D.B., Jilk, R.A., Pollock, S.M., and Marks, M.D. (1998). Control of GL2 expression in Arabidopsis leaves and trichomes. Development **125,** 1161-1171.

Tian, C., Du, Q., Xu, M., Du, F., and Jiao, Y. (2020). Single-nucleus RNA-seq resolves spatiotemporal developmental trajectories in the tomato shoot apex**,** 2020.2009.2020.305029.

Tian, H., Wabnik, K., Niu, T., Li, H., Yu, Q., Pollmann, S., Vanneste, S., Govaerts, W., Rolčík, J., Geisler, M., Friml, J., and Ding, Z. (2014). WOX5–IAA17 Feedback Circuit-Mediated Cellular Auxin Response Is Crucial for the Patterning of Root Stem Cell Niches in Arabidopsis. Molecular plant **7,** 277-289.

Tissier, A. (2018). Plant secretory structures: more than just reaction bags. Current opinion in biotechnology **49,** 73-79.

Turing, A.M. (1990). The chemical basis of morphogenesis. Bulletin of mathematical biology **52,** 153-197.

Walker, J.D., Oppenheimer, D.G., and, J.C., and Larkin, J.C. (2000). SIAMESE, a gene controlling the endoreduplication cell cycle in Arabidopsis thaliana trichomes. Development **127,** 3931-3940.

Wang, K., Ndathe, R.W., Kumar, N., Zeringue, E.A., Kato, N., and Larkin, J.C. (2020). The CDK Inhibitor SIAMESE Targets Both CDKA;1 and CDKB1 Complexes to Establish Endoreplication in Trichomes. Plant physiology **184,** 165-175.

Wang, Y.-L., Nie, J.-t., Chen, H.-M., Guo, C.-l., Pan, J., He, H.-L., Pan, J.-S., and Cai, R. (2016). Identification and mapping of Tril, a homeodomain-leucine zipper gene involved in multicellular trichome initiation in Cucumis sativus. Theoretical and Applied Genetics **129,** 305-316.

Wenkel, S., Emery, J., Hou, B.-H., Evans, M.M.S., and Barton, M.K. (2007). A Feedback Regulatory Module Formed by LITTLE ZIPPER and HD-ZIPIII Genes. The Plant cell **19,** 3379-3390.

Werner, T.s., Motyka, V.c., Laucou, V.r., Smets, R.l., Van Onckelen, H., and Schmu¨lling, T. (2003). Cytokinin-Deficient Transgenic Arabidopsis Plants Show Multiple Developmental Alterations Indicating Opposite Functions of Cytokinins in the Regulation of Shoot and Root Meristem Activity. The Plant cell **15,** 2532-2550.

Wolpert, L., Smith, J.C., Schwab, B., Folkers, U., Ilgenfritz, H., and Hülskamp, M. (2000). Trichome morphogenesis in Arabidopsis. Philosophical Transactions of the Royal Society of London. Series B: Biological Sciences **355,** 879-883.

Wu, J., Sun, W., Sun, C., Xu, C., Li, S., Li, P., Xu, H., Zhu, D., Li, M., Yang, L., Wei, J., Hanzawa, A., Tapati, S.J., Uenoyama, R., Miyazaki, M., Rahman, A., and Wu, S. (2023a). Cold stress induces malformed tomato fruits by breaking the feedback loops of stem cell regulation in floral meristem. New Phytologist **237,** 2268-2283.

Wu, M., Chang, J., Han, X., Shen, J., Yang, L., Hu, S., Huang, B.-B., Xu, H., Xu, M., Wu, S., Li, P., Hua, B., Yang, M., Yang, Z., and Wu, S. (2023b). A HD-ZIP transcription factor specifies fates of multicellular trichomes via dosage-dependent mechanisms in tomato. Developmental cell **58,** 278-288.e275.

Wu, M.L., Cui, Y.C., Ge, L., Cui, L.P., Xu, Z.C., Zhang, H.Y., Wang, Z.J., Zhou, D., Wu, S., Chen, L., and Cui, H. (2020). NbCycB2 represses Nbwo activity via a negative feedback loop in tobacco trichome development. Journal of experimental botany **71,** 1815-1827.

Yan, T., Li, L., Xie, L., Chen, M., Shen, Q., Pan, Q., Fu, X., Shi, P., Tang, Y., and Huang, H. (2018). A novel HD-ZIP IV/MIXTA complex promotes glandular trichome initiation and cuticle development in Artemisia annua. New Phytologist **218,** 567-578.

Yan, T., Chen, M., Shen, Q., Li, L., Fu, X., Pan, Q., Tang, Y., Shi, P., Lv, Z., Jiang, W., Ma, Y.N., Hao, X., Sun, X., and Tang, K. (2016). HOMEODOMAIN PROTEIN 1 is required for jasmonate-mediated glandular trichome initiation in Artemisia annua. New Phytologist **213,** 1145-1155.

Yanagisawa, M., Desyatova, A.S., Belteton, S.A., Mallery, E.L., Turner, J.A., and Szymanski, D.B. (2015). Patterning mechanisms of cytoskeletal and cell wall systems during leaf trichome morphogenesis. Nature Plants **1,** 15014.

Yang, C., Li, H., Zhang, J., Luo, Z., Gong, P., Zhang, C., Li, J., Wang, T., Zhang, Y., and Lu, Y.E. (2011). A regulatory gene induces trichome formation and embryo lethality in tomato. Proceedings of the National Academy of Sciences of the United States of America **108,** 11836-11841.

Yoo, S.D., Cho, Y.H., and Sheen, J. (2007). Arabidopsis mesophyll protoplasts: a versatile cell system for transient gene expression analysis. Nature protocols **2,** 1565-1572.

Zhang, C., Mallery, E.L., Schlueter, J., Huang, S., Fan, Y., Brankle, S., Staiger, C.J., and Szymanski, D.B. (2008). Arabidopsis SCARs Function Interchangeably to Meet Actin-Related Protein 2/3 Activation Thresholds during Morphogenesis. The Plant cell **20,** 995-1011.

Zhang, Y., Xu, T., and Dong, J. (2023). Asymmetric cell division in plant development. Journal of integrative plant biology **65,** 343-370.

Zhao, Y., Pfannebecker, K., Dommes, A.B., Hidalgo, O., Becker, A., and Elomaa, P. (2018). Evolutionary diversification of CYC/TB1-like TCP homologs and their recruitment for the control of branching and floral morphology in Papaveraceae (basal eudicots). New Phytologist **220,** 317-331.

Zheng, F., Cui, L., Li, C., Xie, Q., Ai, G., Wang, J., Yu, H., Wang, T., Zhang, J., Ye, Z., and Yang, C. (2021). Hair interacts with SlZFP8-like to regulate the initiation and elongation of trichomes by modulating SlZFP6 expression in tomato. Journal of experimental botany **73,** 228-244.

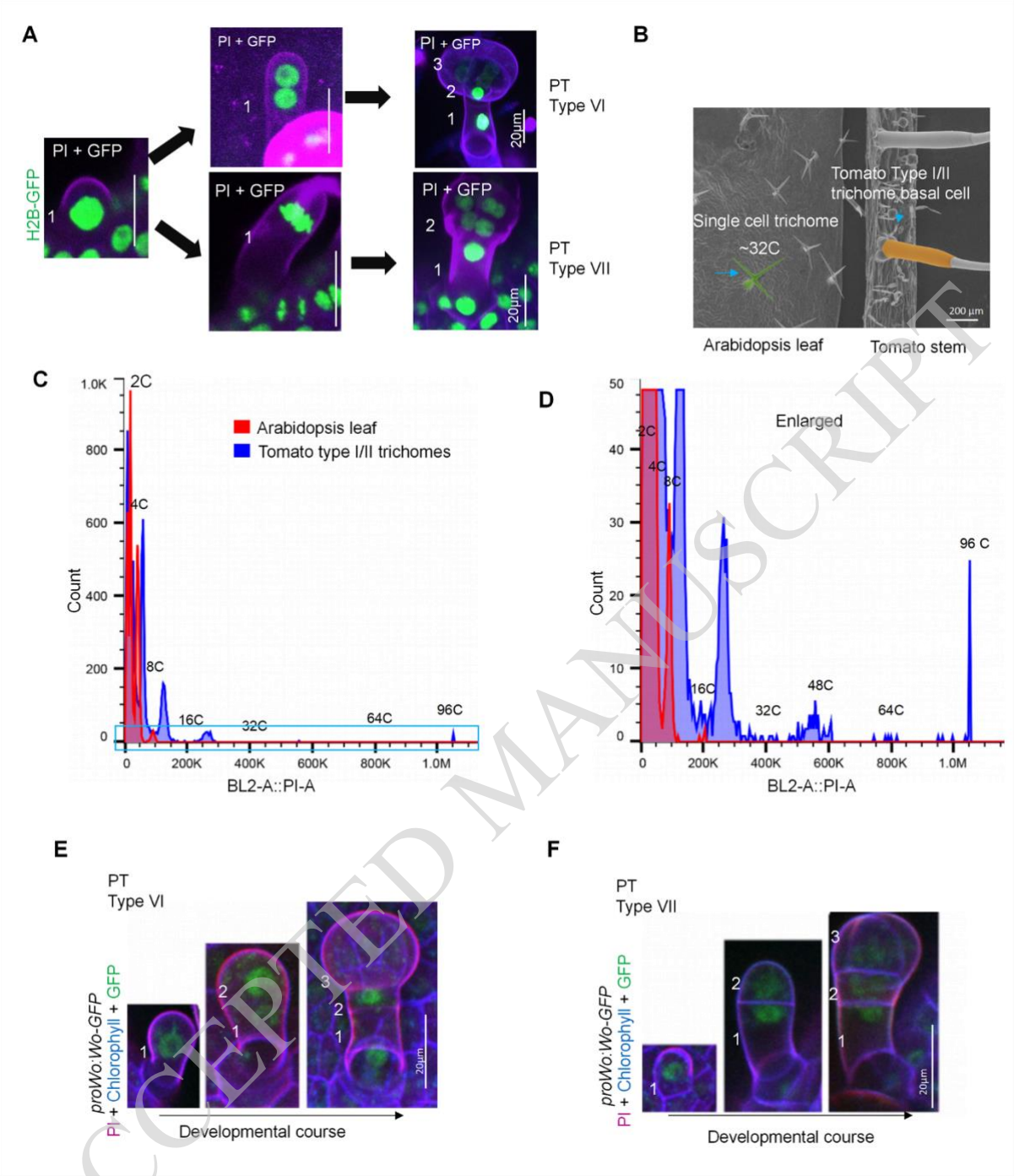

Supplemental Figure S1: Cell division pattern of type VI/VII trichomes and polyploidy state of type I/II trichomes (Supports Figure1 and 2)

A: Confocal images of *pro35S:H2B-GFP* expressing trichomes that are stained with PI (Propidium Iodide). Peltate trichomes (PT) undergo only one round of cell division in the stalk after initiation. Bar=20 μm. **B**: SEM micrographs of tomato type I/II trichomes and *Arabidopsis* trichomes. The nuclei of Arabidopsis trichomes are about 32 C. The basal cell in the mature trichome of tomato was highlighted in orange, and the mature trichome of Arabidopsis was highlighted in green. **C-D**: Flow cytometric analysis of tomato trichomes. **C** is the enlarged view of the area outlined by blue box in **D**. Nuclei from *Arabidopsis* leaves were used as the control. Note the nuclei of tomato

trichomes can reach 96 C. **E-F**: Wo gradient change over the development of type VI (E) and VII (F) trichomes. The number indicates the position relative to the basal cell.

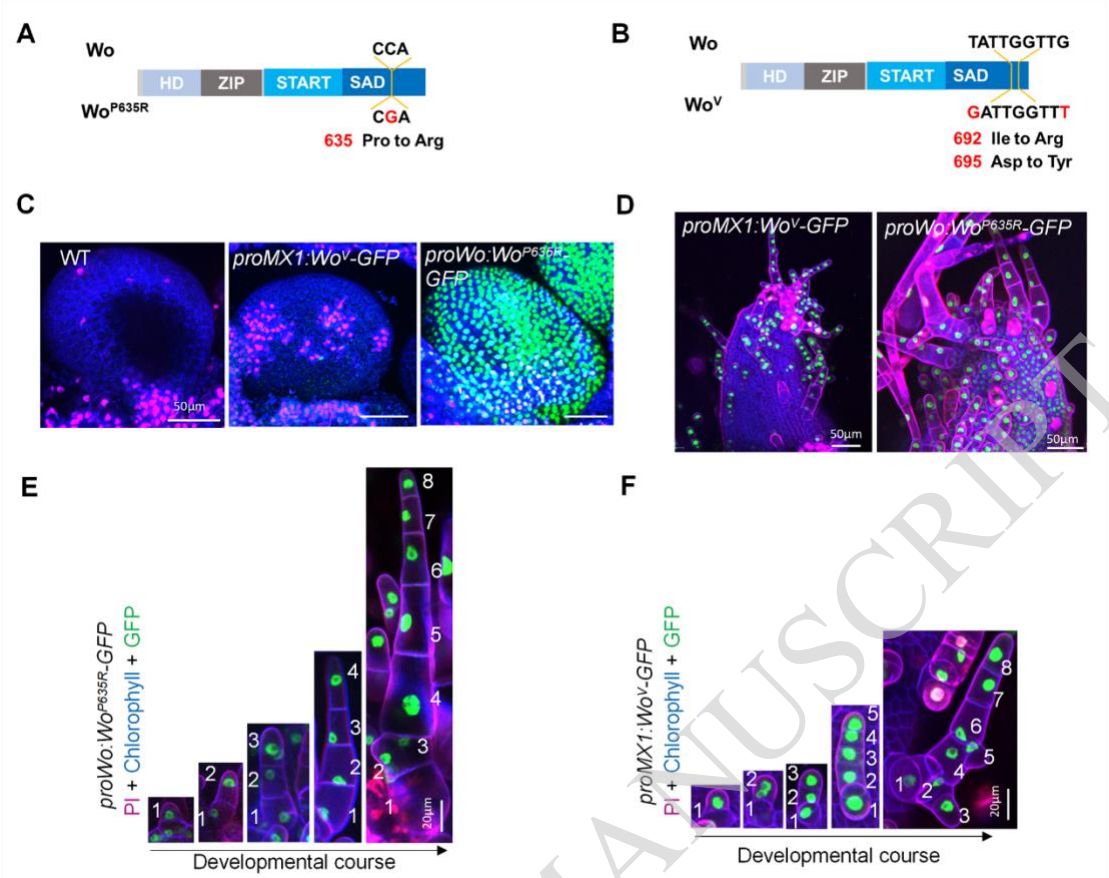

Supplemental Figure S2: The fluorescence pattern of *proMX1:Wo^{V}-GFP* trichomes (Supports Figure 3)

A-B: Schematic representation of Wo^{V} and Wo^{P635R} mutations, two naturally occurring gain-of-function mutations. Wo^{P635R} mutation results in the amino acid shift from proline to arginine at the position 635 of the SAD domain. Wo^{V} mutation results in the amino acid shift from isoleucine to arginine at the position 692 and aspartate to tyrosine at the position 695 of the SAD domain. **C-D**: The expression pattern of Wo^{V}-GFP and Wo^{P635R}-GFP in the ovule epidermis (C) and leaf epidermis (D). Note the *MX1* promoter has a weak expression in the ovule and leaf epidermis compared with Wo promoter, avoiding the strong inhibition of plant growth caused by stabilized Wo^{V} protein. **E-F**: Fluorescence pattern of *proWo:Wo^{P635R}-GFP* (E) and *proMX1:Wo^{V}-GFP* (F) over the development of tomato trichomes. The number indicates the position relative to the basal cell.

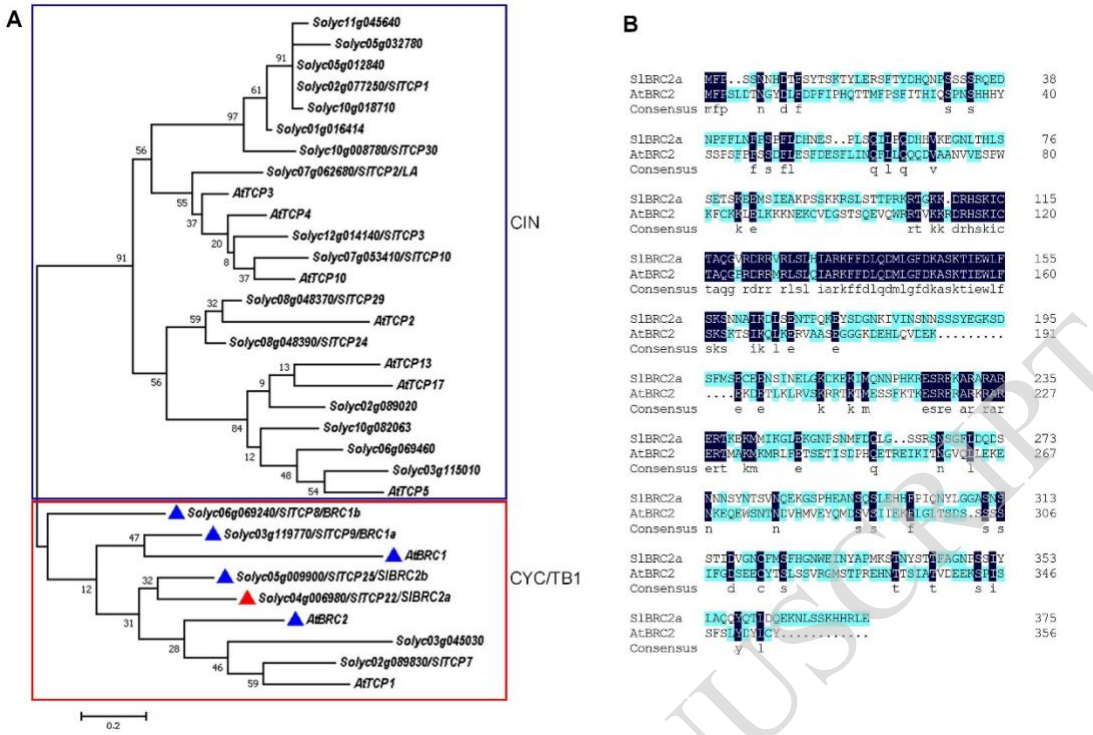

Supplemental Figure S3: Phylogenetic analysis of SlBRC2a protein (Supports Figure 4)

A: A phylogenetic tree of SlBRC2a homologs, which is generated with Maximum Likelihood method. SlBRC2a belongs to the same CYC/TB1 branch as the BRC2 protein. The scale bar indicates the number of substitutions per site. **B:** Protein alignment between SlBRC2a and AtBRC2.

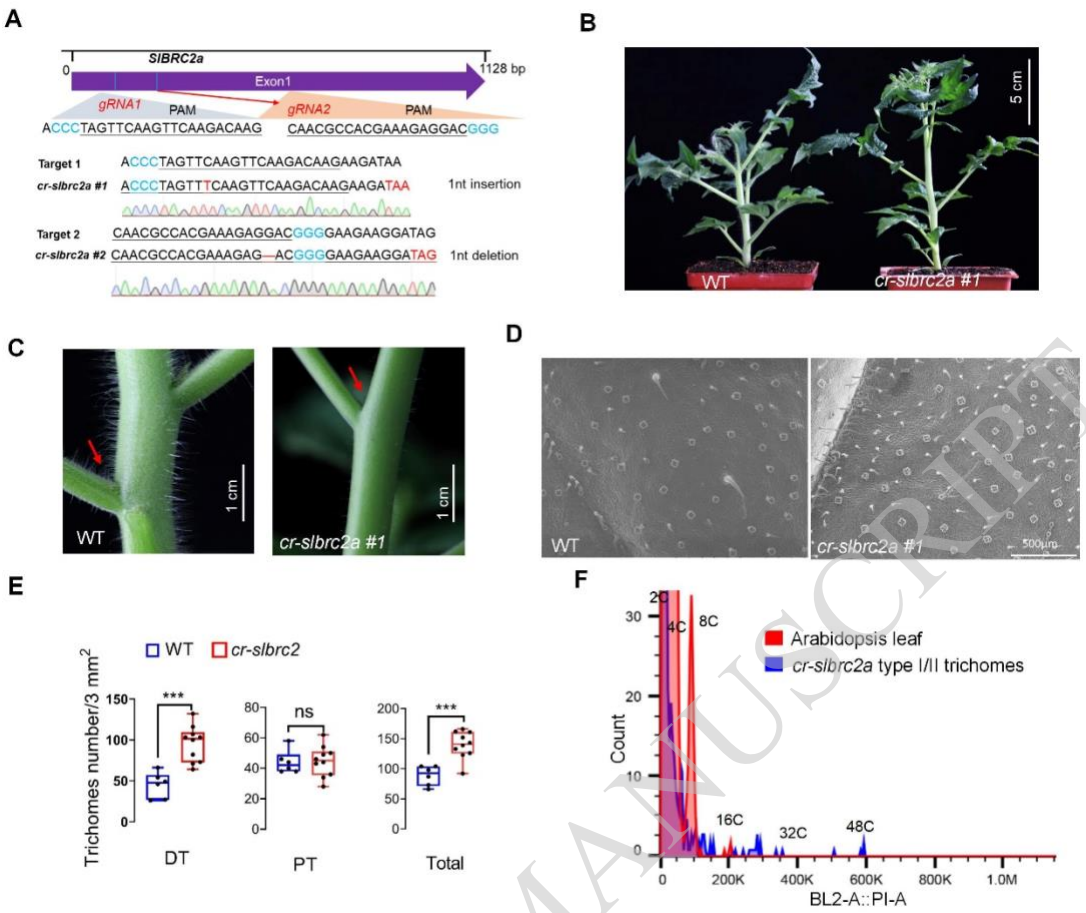

Supplemental Figure S4: *cr-slbrc2a* mutant and phenotype analysis (Supports Figure 4)

A: Schematic diagram of the CRISPR/CAS9 editing targets of *SlBRC2a* gene and the mutations in *cr-slbrc2a* mutant. Both *cr-slbrc2a* #1 and *cr-slbrc2a* #2 cause premature termination of the protein translation. **B:** Phenotype of *cr-slbrc2a* mutant. **C**: Lateral bud phenotype in *cr-slbrc2a* #1 mutant. **D-E:** Trichome phenotype in *cr-slbrc2a* mutant (D). SEM micrographs of *cr-slbrc2a* leaves (D). Quantification of trichome density of *cr-slbrc2a* leaves. Data are mean ± SD (n>10, biological replicates). Note that knockout of the *SlBRC2a* gene results in significantly shorter trichomes in tomato (E). **F**: Flow cytometric analysis of *cr-slbrc2a* trichome nuclei. Nuclei of *Arabidopsis* leaves were used as the control. Note the absence of 96C nuclei in *cr-slbrc2a* trichomes. Unpaired t-tests were used for statistical analysis (***p<0.001, ns: no significant difference).

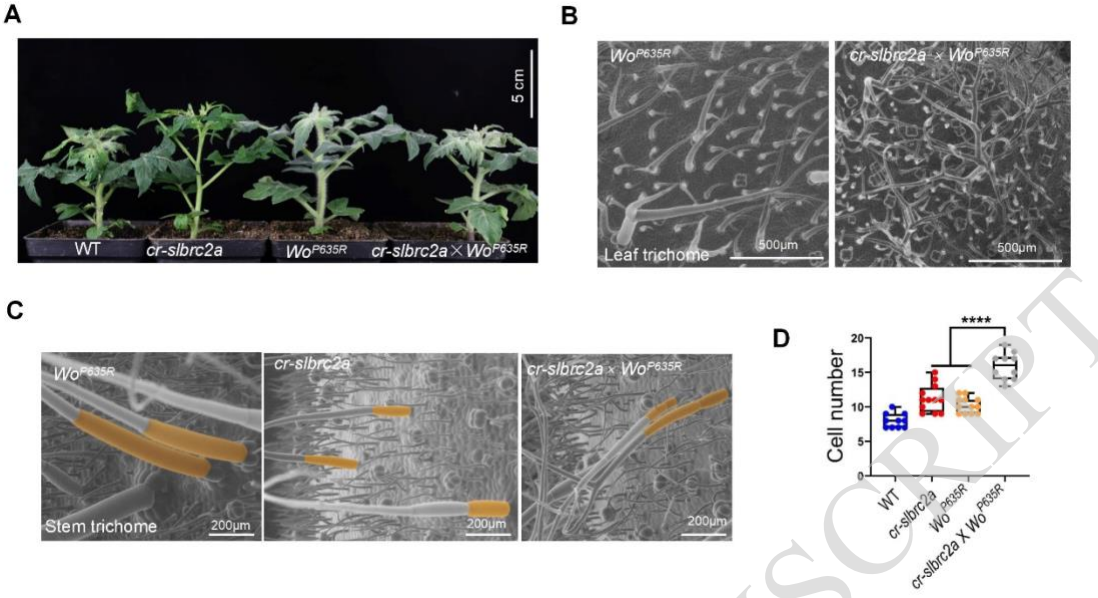

Supplemental Figure S5: Phenotypic analysis of *cr-slbrc2a* × *Wo*^{P635R} plants (Supports Figure 5).

A: Whole plant view of *cr-slbrc2a* × *Wo*^{P635R} double mutants. **B:** SEM micrographs of the trichomes in *cr-slbrc2a* × *Wo*^{P635R} double mutants (leaves). Note that trichome cell division is significantly increased after the knockout of *SlBRC2a* gene in *Wo*^{P635R}. **C:** SEM micrographs of the trichomes in *cr-slbrc2a* × *Wo*^{P635R} double mutants (stems). Note that cell expansion of the basal cells in the type II/II trichomes is significantly reduced after the knockout of the *SlBRC2a* gene in *Wo*^{P635R}. Orange highlights the basal mature cells. **D**: Quantification of the trichome cell number in different backgrounds. Data are mean ± SD (n>10, biological replicates). Unpaired t-tests were used for statistical analysis (****p<0.0001).

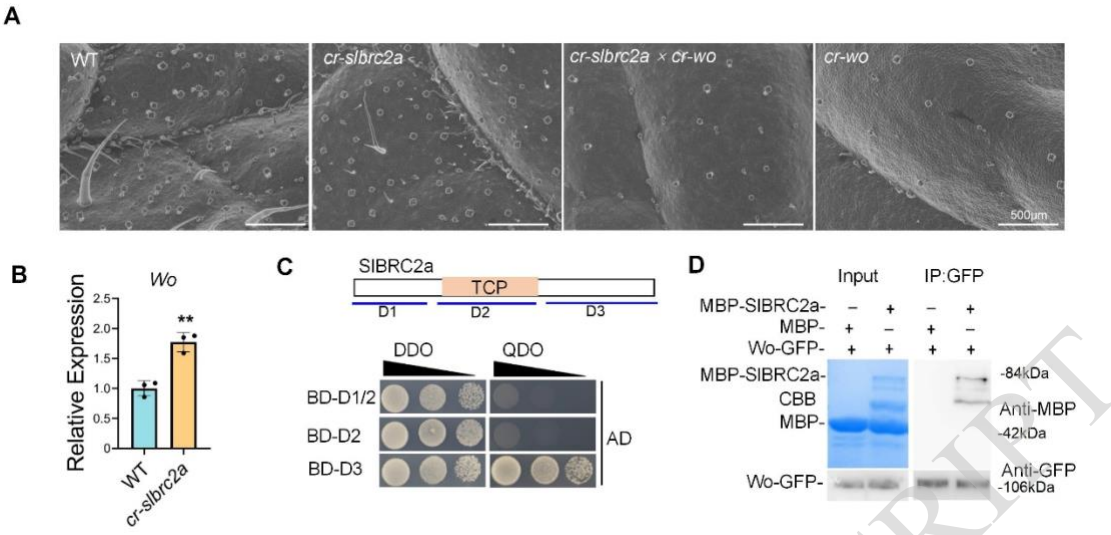

Supplemental Figure S6: Interaction between SlBRC2a and Wo (Supports Figure 6)
A: SEM micrographs showing trichomes in different backgrounds (leaves). **B:** RT-qPCR analysis of *Wo* expression in the trichomes of *cr-slbrc2a* plants. Data are mean ± SD (n=3, biological replicates). **C:** Self-activation of SlBRC2a is detected by Y2H (yeast two-hybrid assay). **D**: The interaction between SlBRC2a and Wo is detected by pull-down assay.

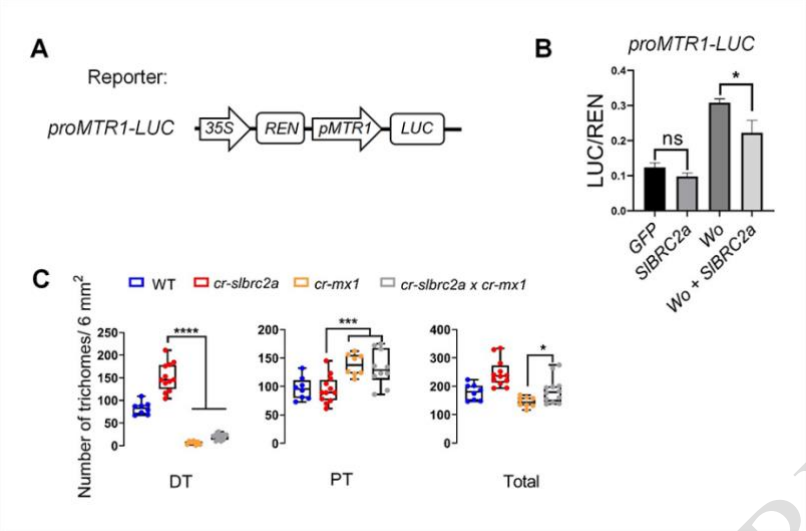

Supplemental Figure S7: SlBRC2a inhibits Wo transcriptional activity (Supports Figure 6)

A-B: LUC reporter assay shows that that the addition of SlBRC2a significantly inhibits the activation of *MTR1* promoter by Wo. Data are mean ± SD (n=3, biological replicates). **C:** Quantification of DT and PT trichome density in different backgrounds. Data are mean ± SD (n>10, biological replicates). Unpaired t-tests were used for statistical analysis (*p<0.05, ***p<0.001, ****p<0.0001, ns: no significant difference). DT: digital trichome, PT: peltate trichome.

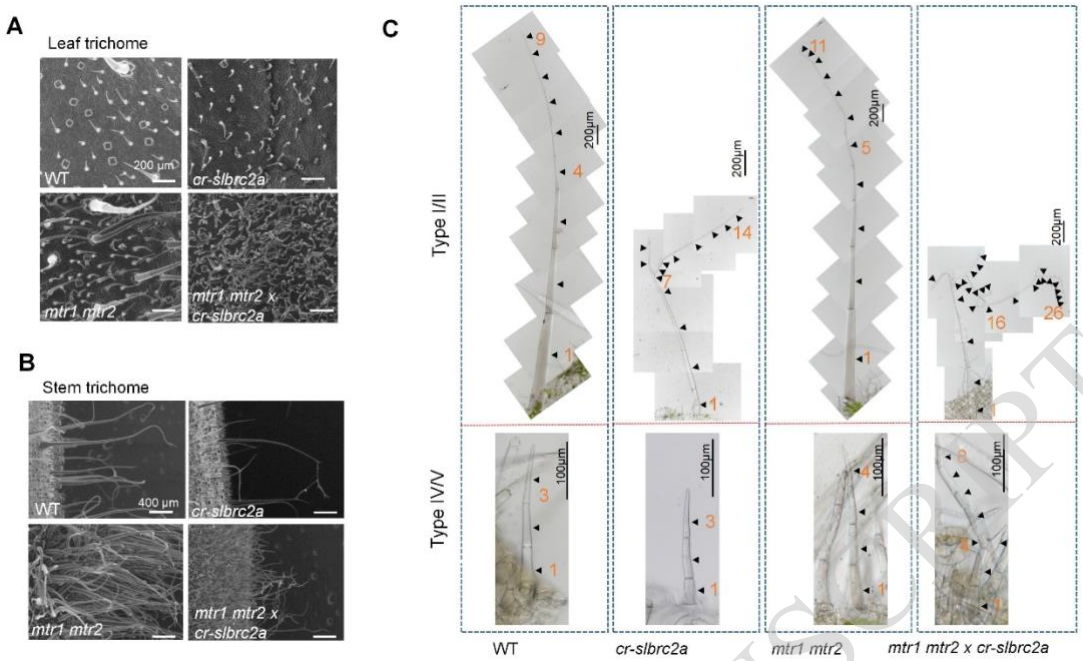

Supplemental Figure S8: Trichome phenotype of *cr-slbrc2a* and *mtr1 mtr2* single, double and triple mutants (Supports Figure 7).

A-B: SEM micrographs of the trichomes in *cr-slbrc2a* and *mtr1 mtr2* single, double and triple mutants. **C:** The DIC images of type I/II and IV/V trichomes in *cr-slbrc2a* and *mtr1 mtr2* single, double and triple mutants. The numbers represent the position of the cell relative to the basal cells. Black triangles point to individual trichome cells.

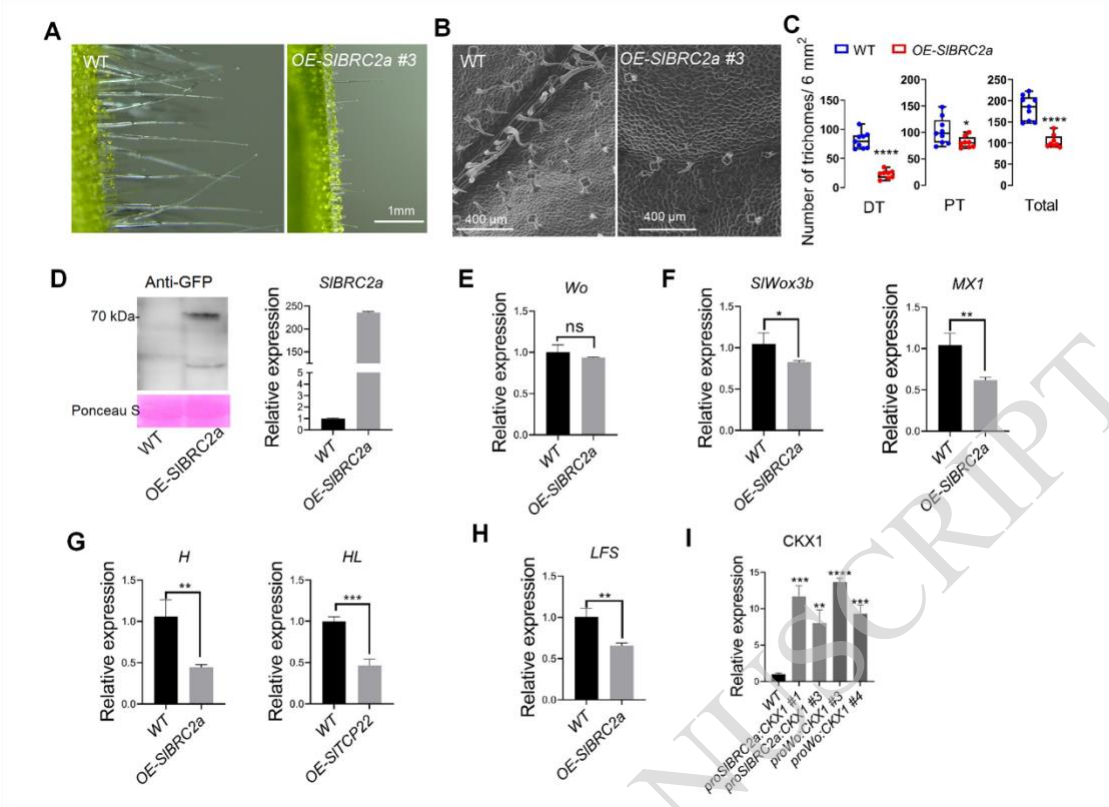

Supplemental Figure S9: SlBRC2a overexpression suppresses downstream gene activation by Wo (Supports Figure 8)

A: Trichome phenotype in WT and *OE-SlBRC2a-GFP* transgenic plants. **B:** SEM micrographs of the trichomes in WT and *OE-SlBRC2a*-GFP transgenic plants. **C:** Quantification of trichome density in WT and *OE-SlBRC2a-GFP* transgenic plants. Data are mean ± SD (n>8, biological replicates). DT: digital trichome, PT: peltate trichome. **D:** Western Blot and RT-qPCR show that *SlBRC2a* levels are increased in *OE-SlBRC2a-GFP* transgenic plants. **E:** RT-qPCR analysis of *Wo* expression in *OE-SlBRC2a-GFP* transgenic plants. Data are mean ± SD (n=3, biological replicates)). **F-H:** RT-qPCR analysis of Wo downstream genes including *SlWox3b*, *MX1*, *H*, *HL* and *LFS* in *OE-SlBRC2a-GFP* transgenic plants. Data are mean ± SD (n=3, biological replicates)). **I:** RT-qPCR analysis of *CKX1* expression in *proSlBRC2a:CKX1-GFP* and *proWo:CKX1-GFP* transgenic plants. Data are mean ± SD (n=3, biological replicates)). Unpaired t-tests were used for statistical analysis (*P<0.05, **P<0.01, ***P<0.001, ****P<0.0001, ns: no significant difference).

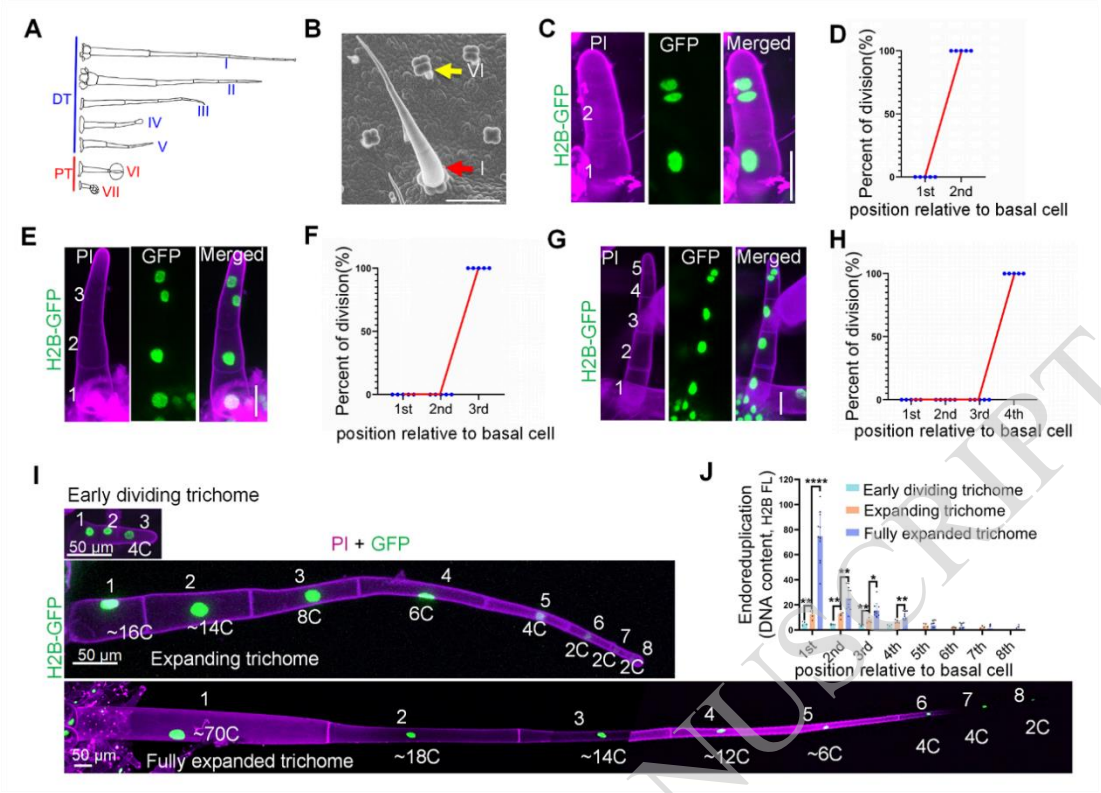

Figure 1. Spatially polarized arrangement of cell division and endoreduplication in tomato trichomes

A: Model of the seven types of tomato trichome. The maximum number of stalk cells is 8-9 for type I/II trichomes, 3-4 for type III trichomes, and 2-3 for type IV/V trichomes, while all peltate trichomes have only one stalk cell. DT: digital trichome, PT: peltate trichome. **B:** Scanning electron micrographs of trichomes on tomato leaves, red arrow is type I trichome and yellow arrow is type VI trichome. The more stalk cells of the trichome, the longer it is. bar = 200 μm. **C-H**: Division positions and statistics of dividing trichomes at different periods with 2, 3 and 4 cells, respectively (n=5, biological replicates). It can be seen from the pictures that the division position of the trichomes in all periods occurred in the most apical cells. Bar = 20 μm. The blue dots represent the percentage of the dividing cells in individual trichomes, and the red lines show the trend of cell division from the bottom to the top of the trichomes. Note that only the top trichome cells divide. **I**: Fluorescence observation of the replication process in the nucleus of tomato trichomes at different developmental stages. H2B-GFP shows the similar size of the nucleus in the early stage of trichome development, and dramatically enlarged nuclear size in the basal cells in more mature stage of trichome development. Bar = 50 μm. **J**: Quantification of nuclear volume of tomato trichomes at different developmental stages. Data are mean ± SD (n>3, biological replicates). Note the polyploidy state of basal cells of mature trichomes can reach up to 70C. Nuclear DNA content is normalized to that of the guard cell. Maximum intensity projection of confocal images of *H2B-GFP* was shown. "H2B FL" represent "H2B-GFP Fluorescence". Unpaired t-tests were used for statistical analysis (*P<0.05, **P<0.01, ****p<0.0001). The number indicates the position relative to basal cell. PI: propidium iodide staining.

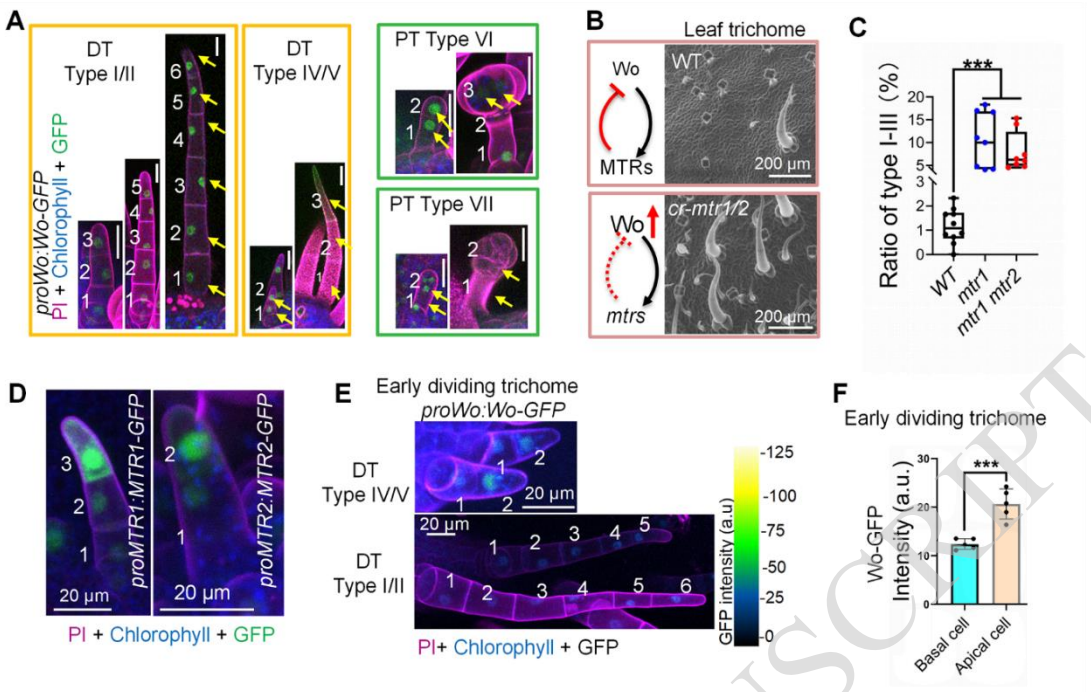

Figure 2. Wo protein gradient is associated with the pattern of division and expansion in tomato trichomes

A: High Wo levels are associated with actively dividing trichome cells. Note the Wo-GFP is seen in all developing trichomes, but gradually disappears in mature trichomes (fully divided type IV/V trichomes and differentiated PT trichomes are shown in this figure). Bar=20 μm. Yellow arrows indicate single cells of a trichome. **B-C:** Higher Wo levels in *mtr1 mtr2* double mutants lead to a significant increase in the density of type I/II/III trichomes with more stalk cells, probably generated by a higher cell division capacity. Data are mean ± SD(n>8, biological replicates). The diagram illustrates the regulatory relationship between Wo and MTRs. Positive regulations are represented by arrow-headed lines, and negative regulations are represented by bar-headed lines. Invalid regulatory relationships are indicated by dashed lines. Box plots display 2nd and 3rd quartiles and the median, bars indicate 1.5x the interquartile range, and the points represent each individual value. **D:** Expression patterns of MTR1 and MTR2 in developing tomato trichomes. **E-F:** Patterns of Wo protein gradient along trichome axis in developing trichomes, showing the highest Wo levels in apical cells (E). Qualifications of Wo protein concentration in basal and apical cells of trichomes (F). The color scale from dark blue to yellow reflects the intensity of protein concentration from weak to strong. Data are mean ± SD (n=5, biological replicates), unpaired t-tests were used for statistical analysis(***P<0.001). The number indicates the position relative to the basal cell. DT: digital trichome, PT: peltate trichome, WT: wild type (Micro-Tom), PI: propidium iodide staining, a.u.: absorbance unit.

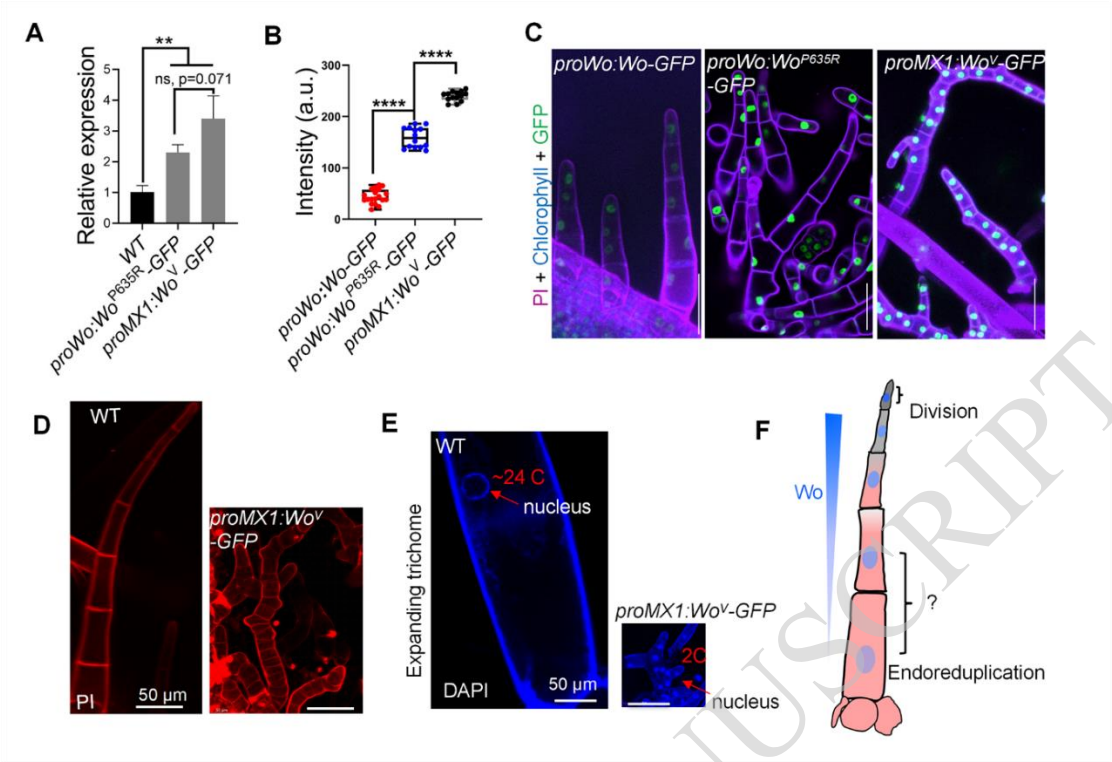

Figure 3. Increased Wo concentration promotes cell division in tomato trichomes

A: RT-qPCR analysis of Wo expression in two-week-old WT, *proWo:Wo^{P635R}-GFP* and *proMX1:Wo^{V}-GFP* seedlings. Total RNA was extracted from young leaves near the SAM. Data are mean ± SD (n=3, biological replicates) **B:** Quantification of fluorescence intensity of GFP-tagged Wo protein in the trichomes of 2-week-old WT (*proWo:Wo-GFP*), *proWo:Wo^{P635R}-GFP* and *proMX1:Wo^{V}-GFP*. Data are mean ± SD (n>14, biological replicates). Box plots display 2nd and 3rd quartiles and the median; bars indicate 1.5x the interquartile range; points represent each individual value. **C:** Confocal images showing the trichome cell division phenotype in two-week-old WT (*proWo:Wo-GFP*), *proWo:Wo^{P635R}-GFP* and *proMX1:Wo^{V}-GFP* plants. Note the promoted trichome cell division induced by enhanced Wo protein stability. Bar = 50μm. **D:** Mature trichomes from WT and *proMX1:Wo^{V}-GFP* lines. Note the dramatically increased cell division in *proMX1:Wo^{V}-GFP* trichomes in which cells do not enter endoreduplication. **E:** DAPI staining of *proMX1:Wo^{V}-GFP* and WT trichomes. Note the nucleus of the WT basal cells reached 24 C, whereas almost all cells have 2C nucleus in the *proMX1:Wo^{V}-GFP* trichomes. **F:** Diagram showing the Wo protein gradient determines the polarized cell division and cell expansion during tomato trichome development. Wo protein maintains high concentration in the apical trichome cells, leading to active cell division in these cells. Reduced Wo concentration in the basal cells allows for endoreduplication in these cells. Additional unidentified factors may be involved in the transition from cell division to endoreduplication. Blue gradients represent the change of Wo concentration. Pink highlights the region of endoreduplication, and gray highlights the region of cell division. Unpaired t-tests were used for statistical analysis (**P<0.01, ****P<0.0001, ns means no significance). WT: wild type (Micro-Tom), PI: propidium iodide staining, a.u.: absorbance unit.

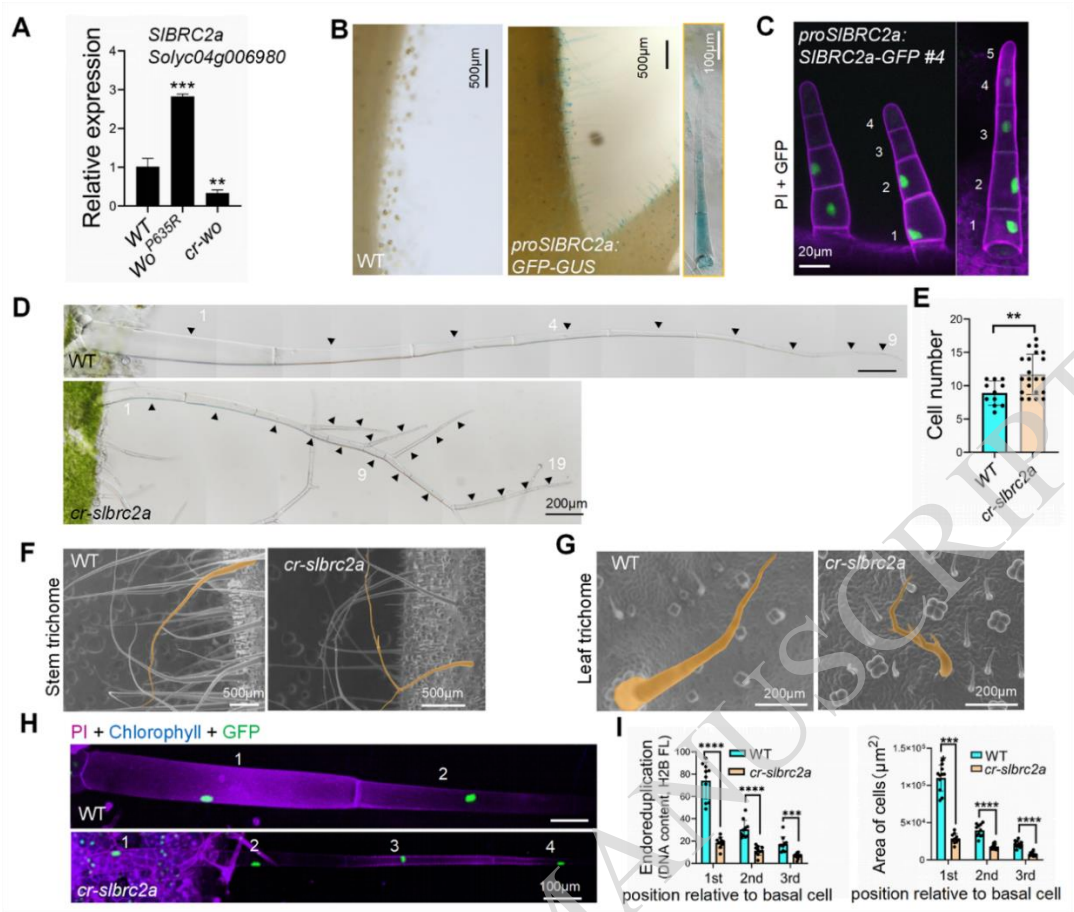

Figure 4. SlBRC2a is a key regulator of the shift to cell expansion in basal cells

A: RT-qPCR analysis of *SlBRC2a* expression in the gain-of-function *Wo* mutant (*Wo*^{P635R}) and loss-of-function mutant (*cr-wo*). Total RNA was extracted from young leaves near SAM. Data are mean ± SD (n=3, biological replicates). **B-C:** Spatial expression pattern of *SlBRC2a* in trichomes. GUS staining of *proSlBRC2a:GFP-GUS* (B) and confocal micrographs of *proSlBRC2a:SlBRC2a-GFP* (C). Note the *SlBRC2a* gene is expressed mainly in basal cells of trichomes. **D-E:** Knockout of *SlBRC2a* gene (*cr-slbrc2a*) causes increased cell division in tomato trichomes. DIC images showing trichomes on the stem of *cr-slbrc2a* plants (D). Quantification of cell numbers in type I/II trichomes (E). Data are mean ± SD(n>10, biological replicate*s).* The black triangles indicate individual cells of trichome. **F-G:** SEM micrographs showing type I/II trichomes in WT and *cr-slbrc2a* mutants. Note the increased cell division and forked trichomes in *cr-slbrc2a* mutants. The phenotypes were most pronounced in the long DT (type I/II) with higher Wo protein concentration. Orange highlights a single mature trichome in the stem and leaf. **H - I**: Quantification of the nucleus size of type I/II trichomes in different backgrounds. Note the significantly reduced cell size and nuclear size in the basal trichome in *cr-slbrc2a* mutants. The quantification indicates that the nucleus size of the first basal cells is 50 C - 100 C in WT, but declines to 10 C – 24 C in *cr-slbrc2a* mutants (I). PI: propidium iodide staining. Nuclear DNA content is normalized to that of the guard cells. Data are mean ± SD(n>10, biological replicates). "H2B FL" presented "H2B-GFP Fluorescence". Unpaired t-tests were used for statistical analysis (**P<0.01, ***P<0.001, ****P<0.0001). The number indicates the position relative to basal cell. WT: wild type (Micro-Tom).

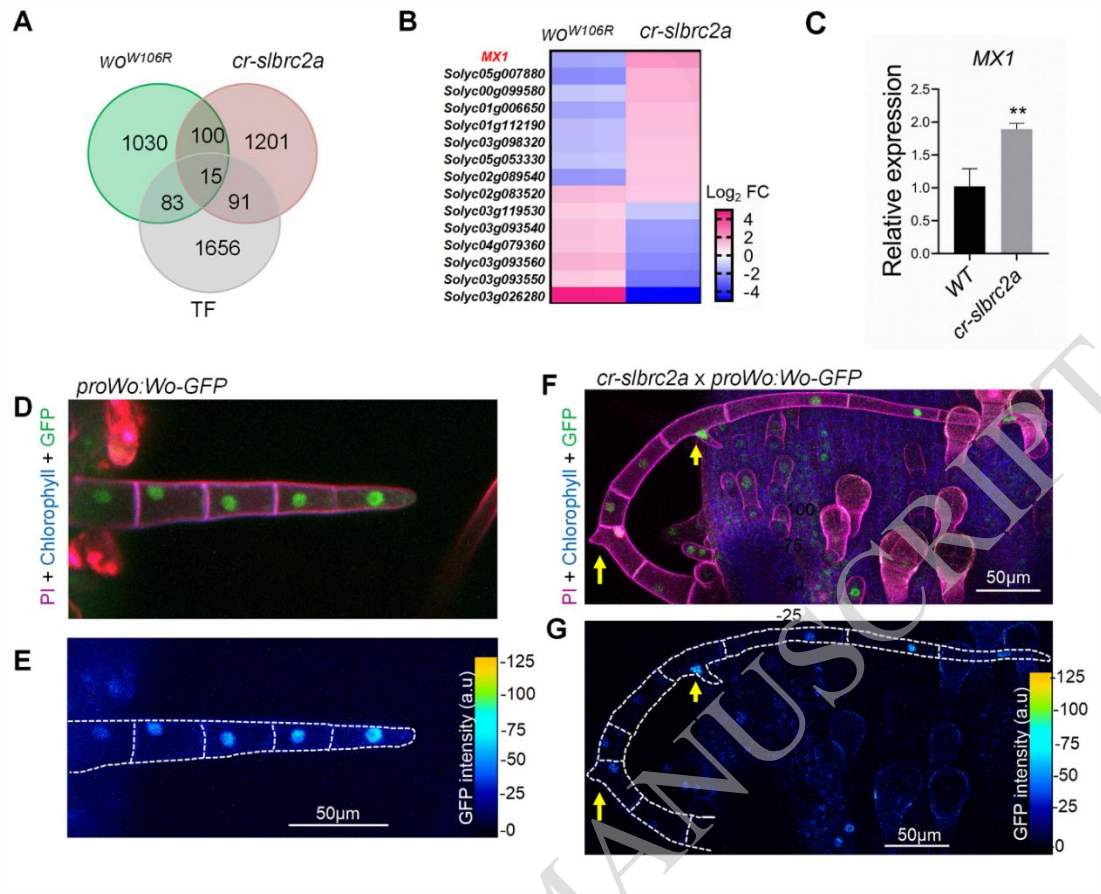

Figure 5. SlBRC2a negatively affects Wo ability of promoting cell division

A: Venn diagram showing the overlap of differentially expressed transcription factors in *cr-slbrc2a* mutants and the loss-of-function mutant *wo*^{W106R}. Transcriptome analysis used stem tissue near the SAM region. TF: transcription factors. **B:** Heat map of differentially expressed transcription factors from the transcriptome analyses. Note the almost opposite expression pattern of the transcription factors in *cr-slbrc2a* and *wo*^{W106R} mutants. The color scale from blue to magenta reflects down-regulation to up-regulation of gene expression level showed by the value of $\log_2$ fold change ($\log_2$ FC). **C:** RT-qPCR analysis of *MX1* expression in *cr-slbrc2a* and WT trichomes. Data are mean ± SD (n=3, biological replicates). Unpaired t-tests were used for statistical analysis (**P<0.01). **D-G:** Confocal images showing Wo-GFP expression pattern in type I/II trichomes of WT and *cr-slbrc2a* × *proWo:Wo-GFP* plants, the yellow arrows indicate dividing cells. **E** and **G** are outlined images shown in **D** and **F** respectively. Note the Wo protein gradient is disrupted when the *SlBRC2a* gene is knocked out. In *cr-slbrc2a* trichomes, bulging is often observed in the dividing basal cells where Wo protein levels are significantly higher. The color scale from dark blue to yellow reflects the intensity of protein concentration from weak to strong. PI: propidium iodide staining.

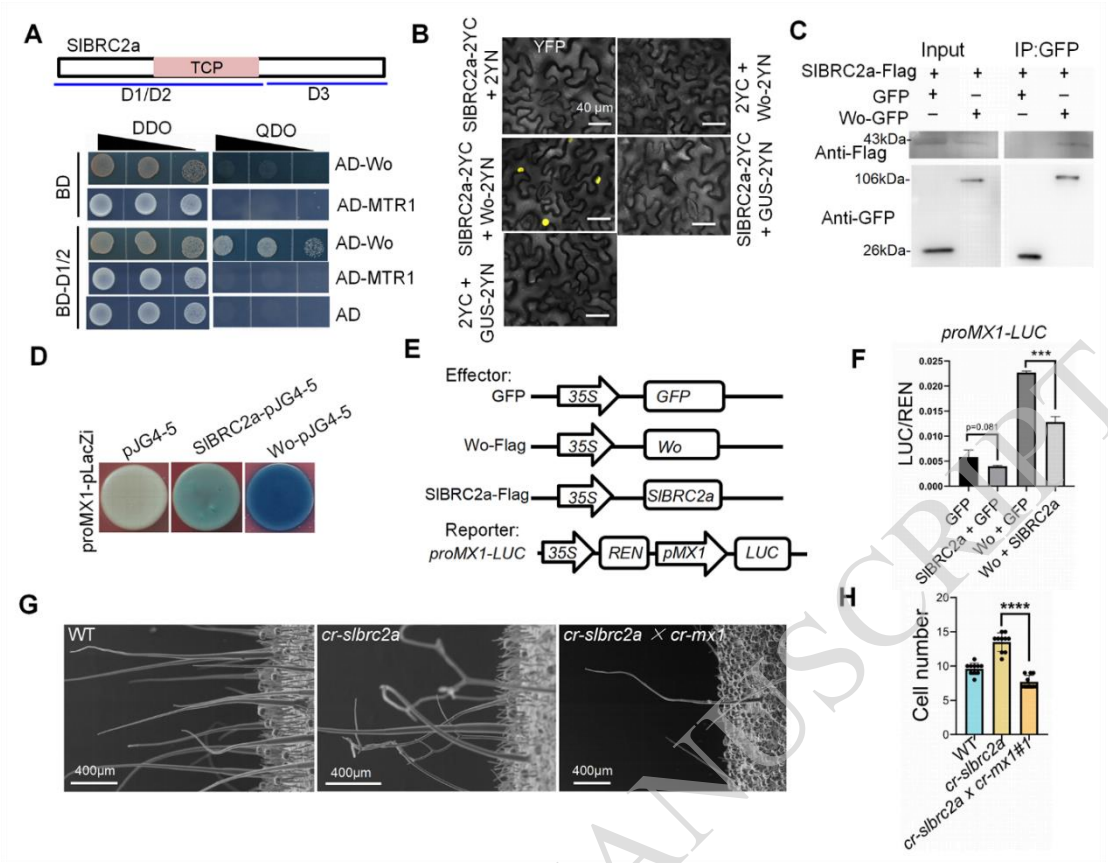

Figure 6. Interaction with SlBRC2a inhibits the transcriptional activity of Wo

A: SlBRC2a interaction with Wo shown by Y2H assay. Due to strong self-activation, SlBRC2a protein is truncated into three segments for Y2H. Both D1 and D2 segments show the interaction with Wo. DDO: double drop out medium (SD/–Leu/–Trp), QDO: quadruple drop out medium (SD/–Ade/–Leu/–His/–Trp). **B:** BiFC verification of SlBRC2a-Wo interaction. **C:** Co-IP validates the interaction between SlBRC2a and Wo. **D:** Y1H assay shows that Wo binds strongly to *MX1* promoter, while SlBRC2a has a weak interaction. **E:** Diagram showing the constructs used in luciferase activation assay (LUC). **F:** LUC assay showing that the addition of SlBRC2a significantly inhibits the activation of *MX1* promoter by Wo. Data are mean ± SD (n=3, biological replicates). **G-H:** *MX1* knockout leads to reduced trichome cell division in *cr-slbrc2a* mutants. SEM micrographs showing the trichome phenotype in different backgrounds (G). Quantification of the cell number of type I/II trichomes in *cr-slbrc2a* and *cr-slbrc2a x cr-mx1* plants (H). Data are mean ± SD (n=10, biological replicates). Unpaired t-tests were used for statistical analysis (***P<0.001, ****P<0.0001).

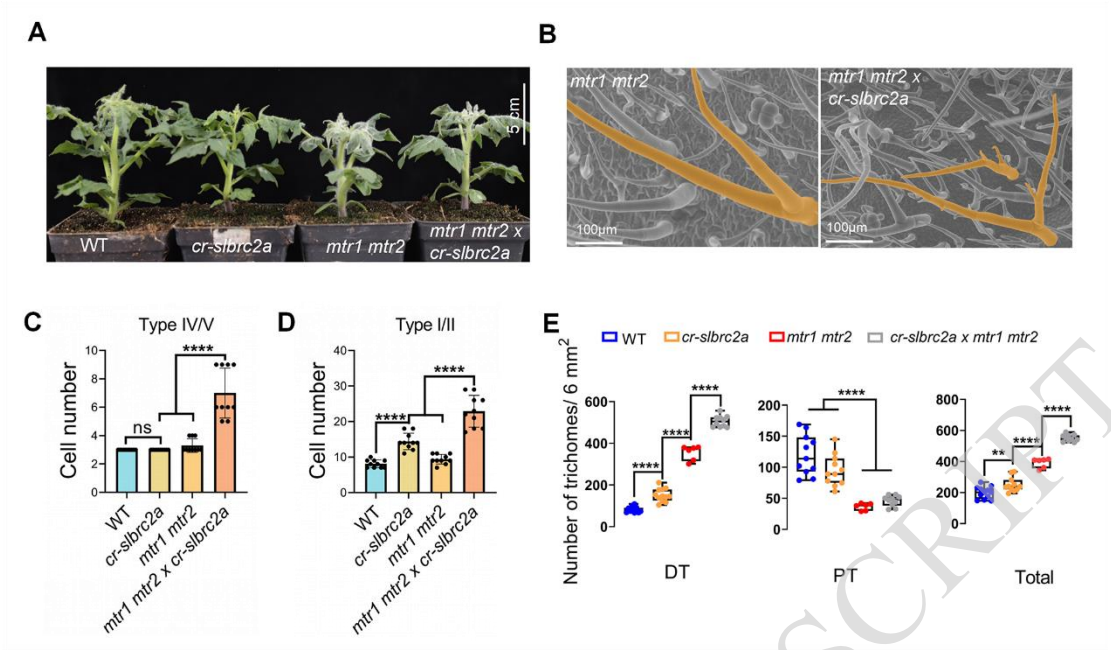

Figure 7. Trichome density and cell division are increased in *MTR1/MTR2/SlBRC2a* triple mutants

A: Phenotype of the single, double and triple mutants of *MTR1, MTR2, SlBRC2a.* **B:** SEM micrographs of the trichomes in *mtr1 mtr2* and *mtr1 mtr2 x cr-slbrc2a* plants. The orange color was used for highlight a single mature trichome. **C-D:** Quantification of the cell number in type IV/V (C) and type I/II (D) trichomes. Data are mean ± SD (n>10, biological replicates) **E:** Quantification of the leaf trichome density. Data are mean ± SD (n>10, biological replicates). Unpaired t-tests were used for statistical analysis (**P<0.01, ****P<0.0001). Box plots display 2nd and 3rd quartiles and the median; bars indicate 1.5x the interquartile range; points represent each individual value. DT: digital trichome, PT: peltate trichome**.** WT: wild type (Micro-Tom).

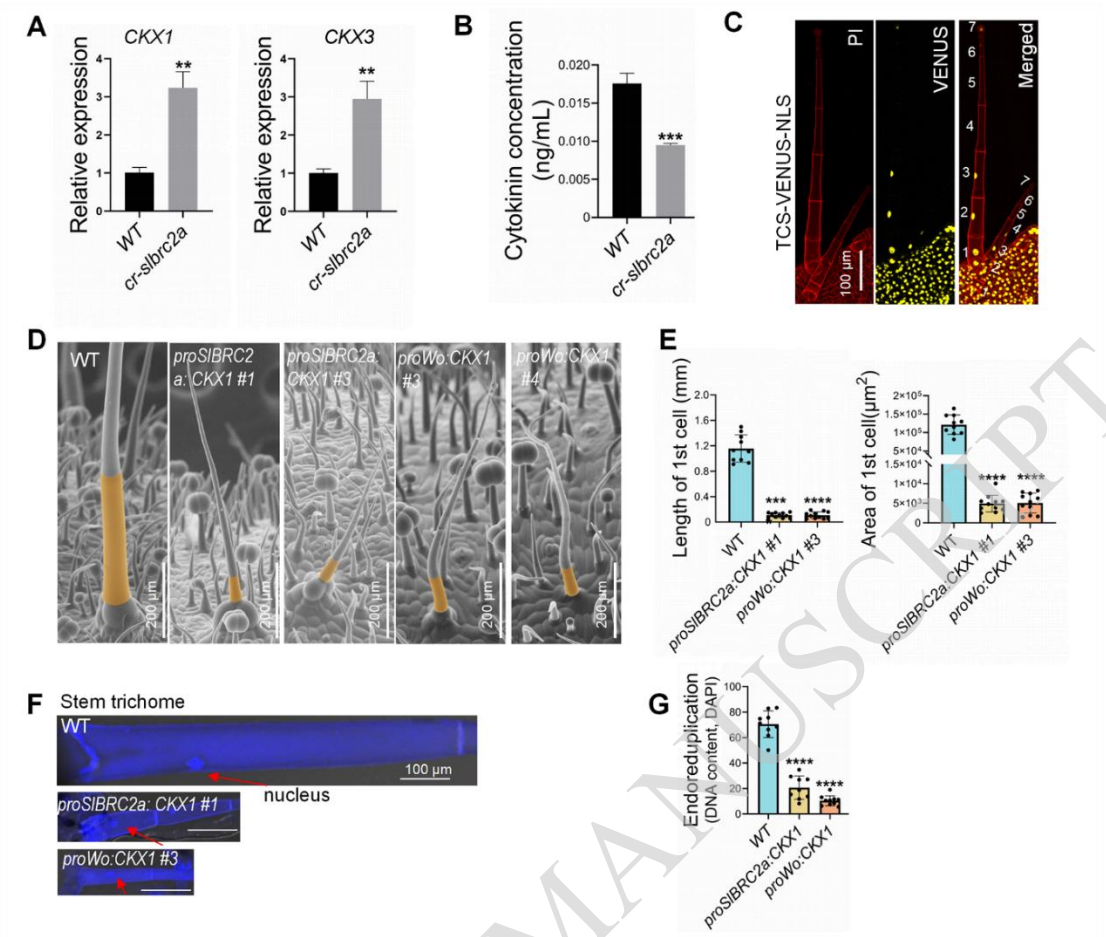

Figure 8. SlBRC2a promotes cell expansion via suppressing *CKX* gene in basal cells

A: RT-qPCR showing *CKX1* and *CKX3* expression in WT and *cr-slbrc2a* trichomes. Data are mean ± SD (n=3, biological replicates). **B:** Liquid chromatography analysis of cytokinin concentration in WT and *cr-slbrc2a* trichomes. Data are mean ± SD (n=3, biological replicates). **C:** *TCS:VENUS-NLS* showing a gradient pattern of cytokinin along trichome axis. The number indicates the position relative to the basal cell. PI: propidium iodide staining. **D:** SEM micrographs of type I/II trichomes in WT, *proSlBRC2a:CKX1-GFP* and *proWo:CKX1-GFP* transgenic plants. The first basal cells of type I/II trichomes are highlighted in yellow. Note the mis-expressions of *CKX1* expression leads to blocked expansion of basal trichome cells. Orange highlights the first cell at the position relative to the basal cell in the mature trichome. **E:** Quantitation of the first basal cells of type I/II trichomes in *proSlBRC2a:CKX1-GFP* and *proWo:CKX1-GFP* transgenic plants. Data are mean ± SD (n>10, biological replicates). **F-G:** Nuclear size of the first basal cells of type I/II trichomes in *proSlBRC2a:CKX1-GFP* and *proWo:CKX1-GFP* plants shown by DAPI staining. Nuclear DNA content is normalized to that in guard cells (2C). The red arrows indicate the nucleus. Data are mean ± SD (n>10). Unpaired t-tests were used for statistical analysis (**p<0.01, ***P<0.001, ****P<0.0001). WT: wild type (Micro-Tom).

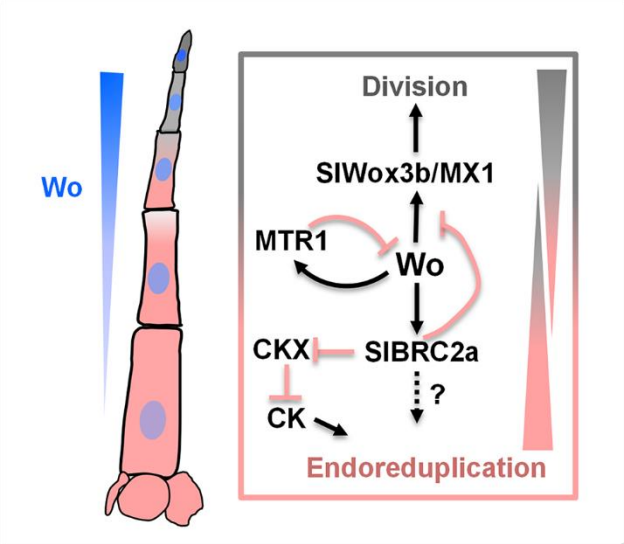

Figure 9. Model of tomato trichome morphogenesis mediated by Wo-SlBRC2a pathway

Wo proteins form a gradient along trichome axis, with the highest Wo concentration in the apical dividing cells. High Wo protein levels promote the cell division of the apical cells by activating the expression of downstream genes including *SlWox3b* and *MX1*. In basal cells, Wo protein level declines, favoring the expression of *SlBRC2a*. SlBRC2a protein in turn binds to Wo proteins, inhibiting Wo transcriptional activity and promoting endoreduplication and cell expansion in basal cells. In basal cells, SlBRC2a contributes to cytokinin accumulation by suppressing the expression of cytokinin-degrading enzyme *CKX1* and *CKX3*. Cytokinin accumulation in basal cells contributes to increased endoreduplication and cell expansion in the basal part of tomato trichomes. In the apical cells, high level of Wo also activates downstream *MTR* genes, which in turn inhibits Wo protein level, forming a negative feedback brake to prevent excessive apical cell division. Blue gradients represent the change of Wo concentration. Pink highlights the region of endoreduplication, and gray highlights the region of cell division. Arrow-headed lines represent positive regulations, and bar-headed lines represent negative regulations. Dashed line with question mark represents hypothesized regulatory relationship. CKX: cytokinin oxidase/dehydrogenase, CK: cytokinin.